

UC Irvine

UC Irvine Previously Published Works

Title

A phosphatidic acid-binding lncRNA SNHG9 facilitates LATS1 liquid-liquid phase separation to promote oncogenic YAP signaling

Permalink

<https://escholarship.org/uc/item/67h221q8>

Journal

Cell Research, 31(10)

ISSN

1001-0602

Authors

Li, Rui-Hua
Tian, Tian
Ge, Qi-Wei
[et al.](#)

Publication Date

2021-10-01

DOI

10.1038/s41422-021-00530-9

Peer reviewed

ARTICLE



A phosphatidic acid-binding lncRNA *SNHG9* facilitates LATS1 liquid–liquid phase separation to promote oncogenic YAP signaling

Rui-Hua Li^{1,13}, Tian Tian^{2,13}, Qi-Wei Ge^{1,3,13}, Xin-Yu He¹, Cheng-Yu Shi¹, Jun-Hong Li¹, Zhen Zhang¹, Fang-Zhou Liu¹, Ling-Jie Sang¹, Zuo-Zhen Yang¹, Ya-Zhuo Liu¹, Yan Xiong⁴, Qingfeng Yan¹, Xu Li⁵, Huai-Qiang Ju^{1,2}, Jian Liu^{6,7}, Liang-Jing Wang³, Jian-Zhong Shao¹, Wenqi Wang⁸, Tianhua Zhou^{3,9,10} and Aifu Lin^{1,10,11,12}✉

© CEMCS, CAS 2021

Long noncoding RNAs (lncRNAs) are emerging as a new class of important regulators of signal transduction in tissue homeostasis and cancer development. Liquid–liquid phase separation (LLPS) occurs in a wide range of biological processes, while its role in signal transduction remains largely undeciphered. In this study, we uncovered a lipid-associated lncRNA, small nucleolar RNA host gene 9 (*SNHG9*) as a tumor-promoting lncRNA driving liquid droplet formation of Large Tumor Suppressor Kinase 1 (LATS1) and inhibiting the Hippo pathway. Mechanistically, *SNHG9* and its associated phosphatidic acids (PA) interact with the C-terminal domain of LATS1, promoting LATS1 phase separation and inhibiting LATS1-mediated YAP phosphorylation. Loss of *SNHG9* suppresses xenograft breast tumor growth. Clinically, expression of *SNHG9* positively correlates with YAP activity and breast cancer progression. Taken together, our results uncover a novel regulatory role of a tumor-promoting lncRNA (i.e., *SNHG9*) in signal transduction and cancer development by facilitating the LLPS of a signaling kinase (i.e., LATS1).

Cell Research (2021) 31:1088–1105; <https://doi.org/10.1038/s41422-021-00530-9>

INTRODUCTION

Previous studies, including ours, indicated that lncRNAs were capable of modulating critical cellular functions and cancer progression.^{1–5} Accumulating studies have shown that cytoplasmic lncRNAs were essential mediators of intracellular signaling pathways, including NF- κ B signaling, HIF-1 α signaling, etc.^{2,6} Our recent study also demonstrated that lncRNAs could naturally associate with the lipid components of the cellular membrane to modulate cellular signaling events. We uncovered a membrane phospholipid PIP3-binding lncRNA, *LINK-A*, which facilitates AKT–PIP3 interaction and consequent AKT enzymatic activation.³ Further delineating the potential properties of lncRNAs in cellular signaling networks will shed light on the discovery of novel therapeutic targets for cancer treatment.

Membraneless compartments formed via active liquid–liquid phase separation (LLPS) or condensation are crucial for spatio-temporal regulation of cellular functions.^{7–9} LLPS is driven by multivalent, weak interactions, involving intrinsically disordered regions (IDR), folded protein, and scaffolding DNA or RNA

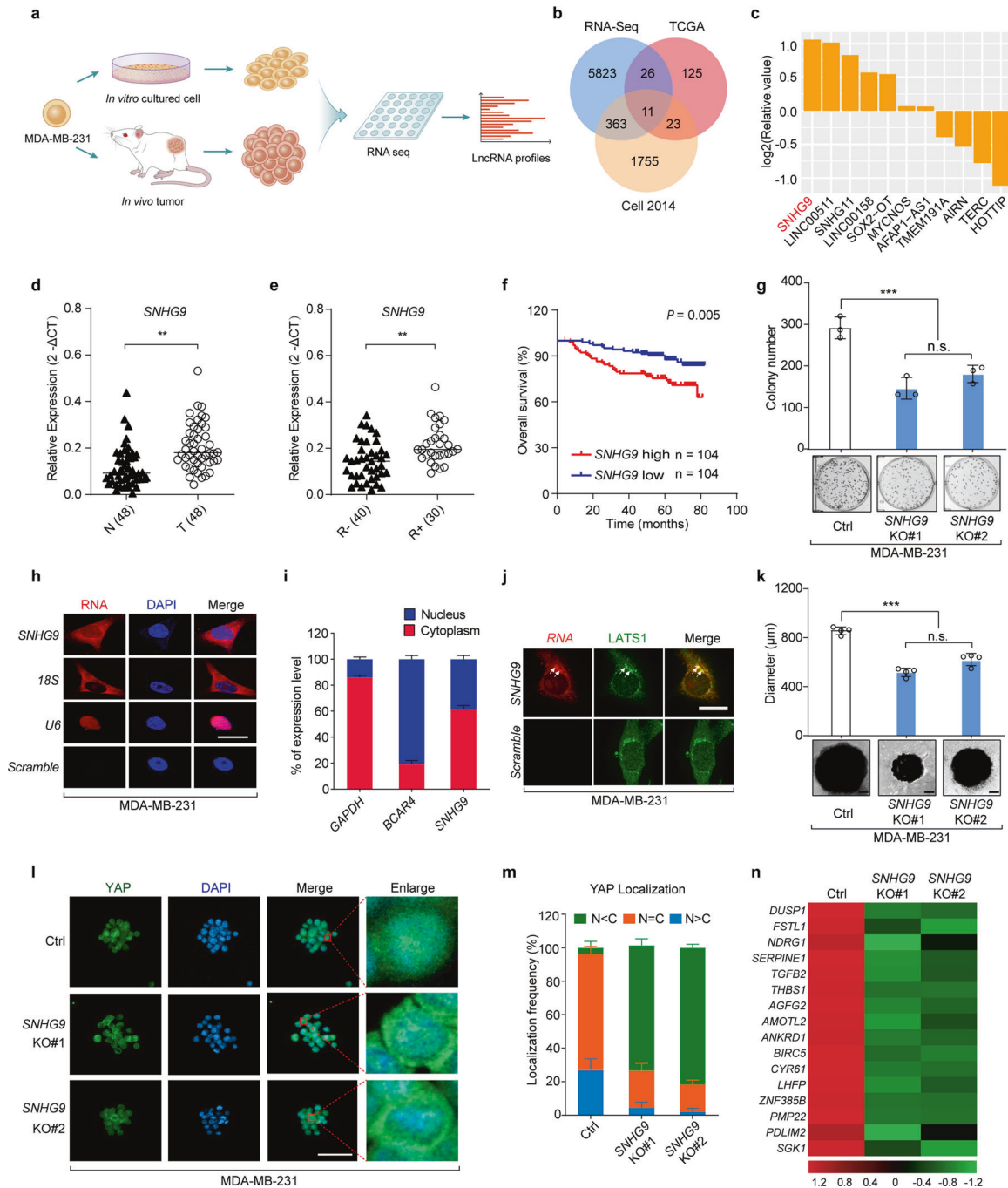
molecules.¹⁰ By coordinating with RNA-binding proteins (RBP), RNAs, such as *NEAT1*,¹¹ also play crucial roles in triggering LLPS in a concentration- or structure-dependent manner.^{12–14} In the nucleus, LLPS is crucial for heterochromatin formation and gene expression regulation.^{15,16} For example, yes-associated protein (YAP) forms liquid-like condensates in the nucleus, which induces the transcription of its target genes.¹⁷ Recent studies indicated that some proteins involved in signal transduction undergo LLPS.^{9,18} For example, DNA-induced phase transition of cGAS promotes its enzyme activity and cGAMP production in innate immune response.⁹ A recent study also indicated that disease-associated mutant SHP2 could recruit and activate wild-type SHP2 in LLPS to promote MAPK kinase hyperactivation.¹⁸ Elucidating the lncRNAs-mediated cytoplasmic phase behaviors will further enrich our understanding of LLPS in signal transduction.

Phosphatidic acids (PA) is a component of membranes and is important for membrane dynamics.^{19,20} There are three major metabolic pathways to produce PA: (1) phospholipase D (PLD) catalyzes the hydrolysis of phosphatidylcholine (PC) to generate

¹MOE Laboratory of Biosystem Homeostasis and Protection, College of Life Sciences, Zhejiang University, Hangzhou, Zhejiang, China. ²Sun Yat-sen University Cancer Center, State Key Laboratory of Oncology in South China, Collaborative Innovation Center for Cancer Medicine, Guangzhou, Guangdong, China. ³Department of Gastroenterology, the Second Affiliated Hospital, School of Medicine and Institute of Gastroenterology, Zhejiang University, Hangzhou, Zhejiang, China. ⁴Department of Orthopedic Surgery, the Second Affiliated Hospital, School of Medicine, Zhejiang University, Hangzhou, Zhejiang, China. ⁵Key Laboratory of Structural Biology of Zhejiang Province, Westlake Laboratory of Life Sciences and Biomedicine, Westlake University, Hangzhou, Zhejiang, China. ⁶Zhejiang University-University of Edinburgh Institute (ZJU-UoE Institute), Zhejiang University School of Medicine, International Campus, Zhejiang University, Haining, Zhejiang, China. ⁷Department of Respiratory and Critical Care Medicine, the Second Affiliated Hospital, Zhejiang University School of Medicine, Hangzhou, Zhejiang, China. ⁸Department of Developmental and Cell Biology, University of California, Irvine, Irvine, CA, USA. ⁹Department of Cell Biology and Program in Molecular Cell Biology, Zhejiang University School of Medicine, Hangzhou, Zhejiang, China. ¹⁰Cancer Center, Zhejiang University, Hangzhou, Zhejiang, China. ¹¹Breast Center of the First Affiliated Hospital, School of Medicine, Zhejiang University, Hangzhou, Zhejiang, China. ¹²Key Laboratory for Cell and Gene Engineering of Zhejiang Province, Hangzhou, Zhejiang, China. ¹³These authors contributed equally: Rui-Hua Li, Tian Tian, Qi-Wei Ge. ✉email: linaifu@zju.edu.cn

Received: 22 November 2020 Accepted: 3 June 2021

Published online: 15 July 2021



PA; (2) lysophosphatidic acid-acyltransferase (LPAAT) catalyzes the conversion of LPA to PA; (3) diacylglycerol kinase (DGK) phosphorylates DAG to produce PA.²¹ PLD-PA signaling plays an important role in cellular metabolism, tumorigenesis, autophagy, and exocytosis.^{19,22} Additionally, PA produced by PLD interacts with large tumor suppressor kinase 1 (LATS1) to activate YAP activity.²¹

Over the past decades, the Hippo pathway has been demonstrated as a tumor suppressor signaling pathway via restricting its downstream effector, YAP.^{23–26} Dysregulation of the Hippo pathway is associated with a broad spectrum of cancers.^{24,27,28} In mammalian systems, MST1/2 phosphorylate and activate LATS1.²⁹ A previous study indicated that PA acts as a key regulator of the Hippo pathway by binding LATS1 to inhibit the formation of the LATS1–MOB1 complex, leading to LATS1

inactivation.²¹ Once phosphorylated at S127 by activated LATS1/2, YAP is sequestered in the cytoplasm by 14-3-3 proteins. Unphosphorylated YAP translocates into the nucleus and associates with TEAD transcription factors to promote transcription of downstream genes. Previous study also showed that lncRNA *MAYA* regulates YAP activity by inhibiting MST1 during bone metastasis.³⁰ However, detailed regulation of lncRNAs and their roles in the Hippo pathway remain largely unknown. Further delineating the lncRNAs involved in the Hippo pathway might provide new insights into physiological hemostasis and human diseases such as cancers.

In this study, we showed that a lipid-associated tumor-promoting lncRNA, small nucleolar RNA host gene 9 (*SNHG9*) is involved in the Hippo pathway regulation. Mechanistically, *SNHG9* and its associated PA bind LATS1 and inhibit LATS1 kinase

Fig. 1 The genome-wide analysis identified a lncRNA *SNHG9* upregulated in breast tumors compared to cultured cancer cells. **a** Schematic illustration showing the analysis of lncRNA profiles from subcutaneously xenografted tumors grown in vivo and tumor cells cultured in dishes in vitro. **b** A Venn Diagram showing upregulated lncRNAs within RNA-seq data, TCGA data (https://ibl.mdanderson.org/tanric/_design/basic/analysis.html) and our previous TNBC profiling data.¹ **c** The list of 11 differentially expressed lncRNAs involved in 3D-cultured cells. **d** qRT-PCR detection of *SNHG9* expression in breast cancer tissues and paired adjacent normal tissues ($n = 48$, Sun Yat-sen cohort). Horizontal black lines represent median values (** $P < 0.01$, Student's t -test). **e** qRT-PCR detection of *SNHG9* expression in breast cancer tissues from patients with (R^+ , $n = 30$) or without (R^- , $n = 40$) recurrence (Sun Yat-sen cohorts). Horizontal black lines represent median values (** $P < 0.01$, Student's t -test). **f** Kaplan–Meier survival analysis of *SNHG9* expression in breast cancer patients ($n = 208$, Kaplan–Meier analysis with Gehan–Breslow test, $P = 0.005$). **g** The colony formation assay was performed on wild-type MDA-MB-231 cells and *SNHG9* KO MDA-MB-231 cells. Error bars, SEM of three independent experiments (n.s., not significant; *** $P < 0.001$, Student's t -test). **h** Subcellular localization of RNAs was detected by RNA FISH in MDA-MB-231 cells. Scale bar, 10 μ m. **i** qRT-PCR detection of RNA expression in cytoplasmic and nuclear fractionations of MDA-MB-231 cells. Error bars, SEM of three independent experiments. **j** Spatial analysis of LATS1 and *SNHG9* colocalization. Representative confocal images of LATS1 (green) and *SNHG9* (red) in MDA-MB-231 cells are shown. Scale bar, 10 μ m. **k** In vitro 3D culture and sphere formation assays were performed using wild-type MDA-MB-231 cells and *SNHG9* KO MDA-MB-231 cells. The representative pictures were shown (bottom) and the diameter of the sphere was measured (top). Scale bar, 200 μ m. Error bars, SEM of three independent experiments (n.s., not significant; *** $P < 0.001$, Student's t -test). **l, m** *SNHG9* induces YAP nuclear translocation. YAP subcellular localization was detected in the formed *SNHG9* WT or *SNHG9* KO tumor sphere (**l**). Scale bar, 50 μ m. Cells from ten different fields were randomly selected and quantified for YAP localization (**m**). Error bars, SEM of three independent experiments. **n** qRT-PCR detection of YAP target gene expression. Heatmap shows significant expression changes induced by *SNHG9* KO in MDA-MB-231 cells.

activity by inducing the LLPS of LATS1. Clinically, *SNHG9* expression positively correlates with YAP activation in advanced breast cancers. These findings reveal a cancer-related lncRNA as a crucial regulator of YAP by driving liquid droplet formation of LATS1.

RESULTS

The genome-wide analysis identified a lncRNA *SNHG9* upregulated in breast tumors compared to cultured cancer cells

To identify lncRNAs highly expressed in tumors, RNAs were isolated from MDA-MB-231 cells cultured in dishes and from their derived xenograft tumors, respectively, and then subjected to RNA-seq analysis (Fig. 1a). Here, 6223 differentially expressed lncRNAs between tumors and the in vitro cultured cells were identified (Fig. 1b; Supplementary information, Table S1). To narrow down the identified lncRNA candidates related to triple-negative breast cancer (TNBC) development, we compared them with a group of lncRNAs highly expressed in human breast cancer from The Cancer Genome Atlas Breast Invasive Carcinoma (TCGA-BRCA) dataset and our previously published triple-negative breast cancer dataset¹ (Fig. 1b; Supplementary information, Table S1). This analysis led us to identify 11 overlapped lncRNA candidates, which were further confirmed by experimental validation (Fig. 1c; Supplementary information, Fig. S1a). A hypergeometric test was conducted on these overlaps, showing that they were statistically significant. Among the upregulated lncRNAs, *SNHG9*, a lipid-binding lncRNA,³ was the most upregulated one under the 3D culture condition (Fig. 1c).

SNHG9 is conserved in humans, rhesus monkeys, and mice as indicated by chromosomal localization and genomic context analyses (Supplementary information, Fig. S1c). The secondary structure of *SNHG9* molecules in above species was predicted. They all have one or two conserved loops at the starting sequence (Supplementary information, Fig. S1d–f), which were relatively more conserved among species as compared to other regions (Supplementary information, Fig. S1g).

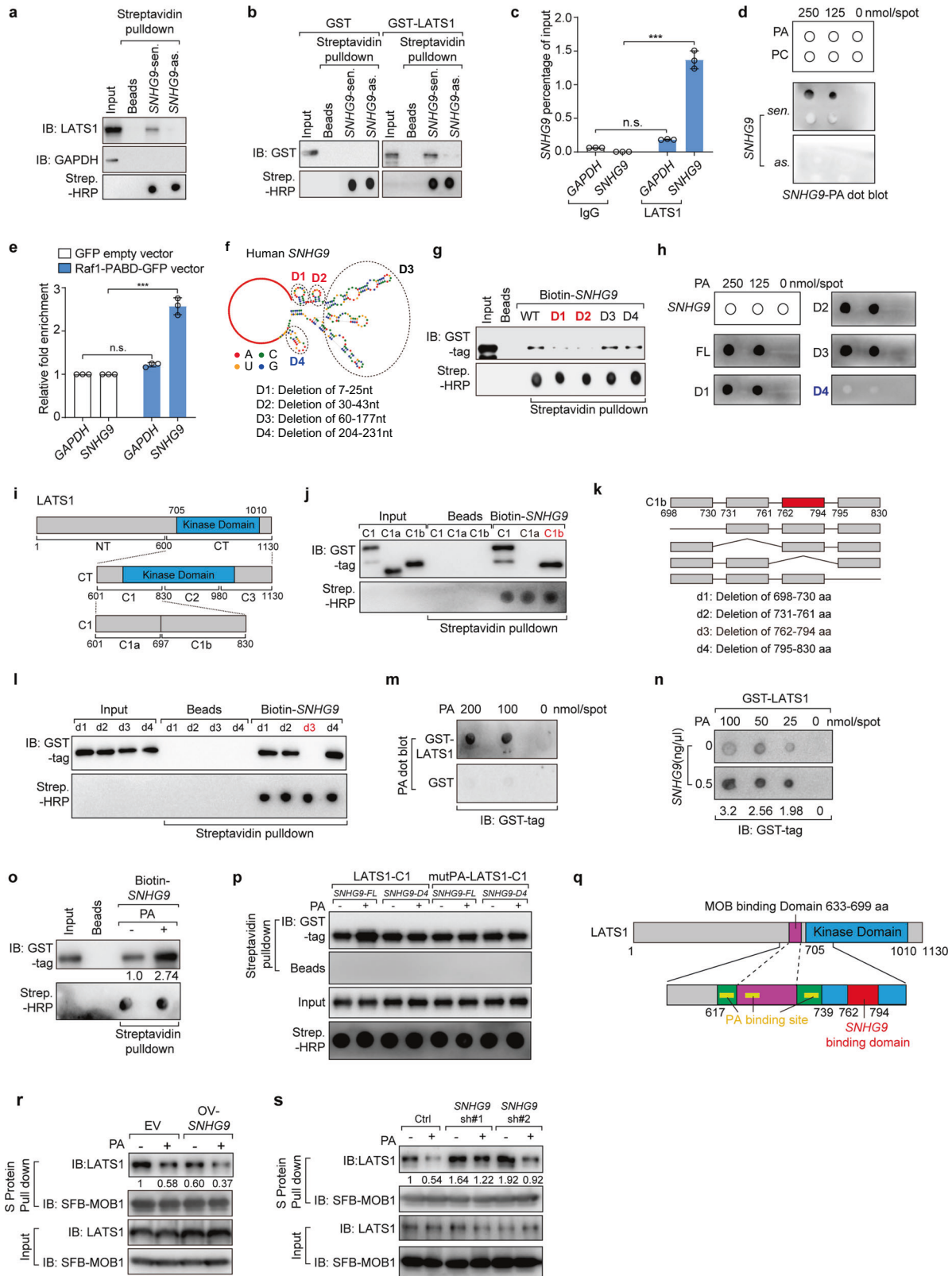
Furthermore, *SNHG9* exhibited a higher expression level in advanced breast cancer tissues from an independent cohort (SYSUCC, $n = 48$) compared with that in the paired control samples (Fig. 1d). Similar findings were observed in multiple cancer types (Supplementary information, Fig. S1b). It also showed a higher expression in TNBC cell lines (e.g., MDA-MB-231 and MDA-MB-468 cells) compared with that in other types of breast cancer cells or mammary epithelial cells (e.g., MCF-10A) (Supplementary information, Fig. S1j). To examine the

capability of *SNHG9* in encoding micropeptides, we conducted a ribosome profiling to detect the enrichment of *SNHG9* in distinct groups of ribosomal polysomes. The results showed that *SNHG9* was barely enriched in the polysome components (fractions 8–11) comparing with the canonical mRNA (*GAPDH*); and the distribution pattern was consistent with the known lncRNA *ACOD1*,³¹ which indicated the incapability of *SNHG9* in encoding micropeptides (Supplementary information, Fig. S1h, i). We further examined the copy number of *SNHG9* in aggressive breast cancer cells, and found that each MDA-MB-231 and MDA-MB-468 cell contains 842 copies and 418 copies, respectively (Supplementary information, Fig. S1k, l). Moreover, breast cancer patients with higher expression levels of *SNHG9* showed unfavorable recurrence-free survival ($n = 30$) and overall survival (SYSUCC, $n = 208$) (Fig. 1e, f). To explore the role of *SNHG9* in breast tumor growth, we generated *SNHG9* knockout (KO) MDA-MB-231 cell line (Supplementary information, Fig. S1m–o) and found that loss of *SNHG9* impaired breast cancer cell anchorage-independent growth (Fig. 1g). These data suggest that *SNHG9* is involved in TNBC development.

Next, we conducted RNA fluorescence in situ hybridization (FISH) and qRT-PCR analyses to examine *SNHG9* expression in MDA-MB-231 cells. We found that *SNHG9* was mainly localized in the cytoplasm (Fig. 1h, i) and co-localized with PA (Supplementary information, Fig. S2a, b), a phospholipid regulator of the Hippo pathway that is known to bind *SNHG9*.^{3,21} We also found that PA co-localized with the Hippo pathway kinase LATS1 (Supplementary information, Fig. S2c, d). Following this finding, we further observed the co-localization between *SNHG9* and LATS1 (Fig. 1j; Supplementary information, Fig. S2e). We next employed a 3D tumor spheroid assay to evaluate the impact of *SNHG9* on tumor cell growth. We found that *SNHG9* KO mutants displayed impaired spheroid formation (Fig. 1k). Interestingly, loss of *SNHG9* increased LATS1 autophosphorylation (S909) and induced YAP S127 phosphorylation (Supplementary information, Fig. S2f) and cytoplasmic translocation (Fig. 1l, m), along with the down-regulation of YAP target gene expression (Fig. 1n). These results suggest that *SNHG9* plays a tumor-promoting role in tumor growth, probably by repressing LATS1 activity.

SNHG9 interacts with PA and LATS1

To elucidate how *SNHG9* regulates LATS1 in breast cancer, we examined the potential *SNHG9*–LATS1 interaction using RNA pull-down assay and RNA immunoprecipitation (RIP) assay. RNA pull-down in cell lysates (Fig. 2a) and in vitro RNA pull-down with bacterially expressed recombinant LATS1 protein (Fig. 2b) showed that *SNHG9* directly interacted with LATS1, and that murine *snhg9*



also bound with LATS1 (Supplementary information, Fig. S3a). The endogenous interaction between *SNHG9* and LATS1 was confirmed using RIP assay in MDA-MB-231 cells (Fig. 2c). In addition, consistent with our previous study,³ *SNHG9* directly bound PA, as indicated by in vitro lipid-RNA dot blotting (Fig. 2d). Using RIP

assay in MDA-MB-231 cells, we also observed the endogenous interaction between PA and *SNHG9* (Fig. 2e).

Analysis of the *SNHG9* secondary structure using the RNAfold software showed it has six loops (Fig. 2f). To map RNA motifs essential for the *SNHG9*-LATS1 and *SNHG9*-PA interactions, we

Fig. 2 *SNHG9* interacts with PA and LATS1. **a** Immunoblot detection of proteins retrieved by in vitro-transcribed *SNHG9* sense (*sen.*) or antisense (*as.*) transcripts from MDA-MB-231 cell lysates. **b** In vitro transcribed biotinylated *SNHG9-sen.* or *SNHG9-as.* transcripts were incubated with indicated recombinant proteins for in vitro RNA pull-down analysis. **c** RIP assays were performed using the indicated antibodies in MDA-MB-231 cell lysates. Error bars, SEM of three independent experiments (n.s., not significant; ****P* < 0.001, Student's *t*-test). **d** PA interacts with *SNHG9*. In vitro-transcribed *SNHG9-sen.* or *SNHG9-as.* transcripts were subjected to the lipid dot-blot assay. PC was used as a negative control. **e** RIP assays were performed using anti-GFP antibody in MDA-MB-231 cells harboring indicated vectors. Error bars, SEM of three independent experiments (n.s., not significant; ****P* < 0.001, Student's *t*-test). **f** The predicted secondary structure of *SNHG9* was made by RNAfold software, and schematic illustration of *SNHG9* mutations used in this study was shown. **g** Immunoblot detection of proteins retrieved by indicated in vitro transcribed biotinylated *SNHG9* deletion mutants from recombinant GST-LATS1-CT. **h** PA binds with the sixth loop of *SNHG9*. In vitro-transcribed *SNHG9* WT and its deletion mutants were subjected to the lipid dot-blot assay. **i** Schematic illustration of LATS1 protein and its truncations used in this study. **j** Two fragments in the C1 (601–830 aa) of LATS1 were named as C1a and C1b. Immunoblot detection of proteins retrieved by in vitro-transcribed biotinylated *SNHG9* from indicated recombinant GST-LATS1-C1 mutants was shown. **k** Schematic illustration of the C1b fragment of LATS1 protein and its deletion mutants. **l** Four deletion mutants in the C1b (698–830 aa) were named as d1, d2, d3 and d4. Immunoblot detection of proteins retrieved by in vitro-transcribed biotinylated *SNHG9* from indicated recombinant GST-LATS1-C1b mutants was shown. **m** PA interacts with LATS1. In vitro-purified GST-LATS1 was subjected to the lipid dot-blot assay. **n** *SNHG9* promotes the interaction between PA and LATS1. In vitro-transcribed *SNHG9* and in vitro-purified GST-LATS1 were subjected to the lipid dot-blot assay. **o** PA increased the levels of *SNHG9*-enriched LATS1. In vitro-transcribed biotinylated *SNHG9* transcripts were incubated with GST-LATS1-CT proteins and 300 μ M PA for in vitro RNA pull-down analysis. Immunoblot detection of GST-LATS1-CT proteins retrieved by in vitro-transcribed biotinylated *SNHG9* was shown. **p** In vitro-transcribed biotinylated *SNHG9-FL* or *SNHG9-D4* transcripts were incubated with GST-LATS1-C1 or GST-mutPA-LATS1-C1 proteins and 300 μ M PA for in vitro RNA pull-down analysis. Immunoblot detection of GST-LATS1-C1 or GST-mutPA-LATS1-C1 proteins retrieved by in vitro-transcribed biotinylated *SNHG9* was shown. **q** Schematic illustration of LATS1 protein with MOB1-, PA- and *SNHG9*-binding domains. **r** Overexpression of *SNHG9* enhances the inhibitory effect of PA on the LATS1–MOB1 complex association. SFB-MOB1 was overexpressed in HEK293A and *SNHG9*-overexpressed HEK293A cells. Serum-starved above cells were treated with PA (100 μ M) for 1 h. S protein beads were used to pull down the transfected SFB-MOB1, and the co-precipitated LATS1 was detected. **s** Knocking down the expression of *SNHG9* attenuated the inhibitory effect of PA on the formation of the LATS1–MOB1 complex. SFB-MOB1 was overexpressed in HEK293A and *SNHG9* KD HEK293A cells. Serum-starved above cells were treated with PA (100 μ M) for 1 h. S-beads were used to pull down the transfected SFB-MOB1, and the co-precipitated LATS1 was detected.

generated several *SNHG9* mutants by deleting different loop regions (Fig. 2f). In vitro RNA–protein binding assay showed that the first and the second loops of *SNHG9* (D1: delete the first loop, 7–25 nt; D2: delete the second loop, 30–43 nt) mediated its interaction with LATS1 (Fig. 2g), and the sixth loop (D4: delete the sixth loop, 204–231 nt) was required for its interaction with PA (Fig. 2h). To map the domains of LATS1 required for its interaction with *SNHG9*, we tested several truncated forms (CT, NT, C1, C2, and C3) of LATS1 protein (Fig. 2i),²¹ and found that the C1 fragment (601–830 aa) was required for the interaction (Supplementary information, Fig. S3b, c). Further mapping of the LATS1 C1 fragment showed that *SNHG9* bound the 762–794 aa region of the LATS1 kinase domain (Fig. 2i–l). To further test whether these kinase domain truncations could fold into stable structures, we performed circular dichroism analysis (CD analysis) to investigate their secondary structure composition. Results indicated that all these truncation mutants were well folded, and that the content of each secondary structure of these mutants does not have much difference (Supplementary information, Fig. S4).

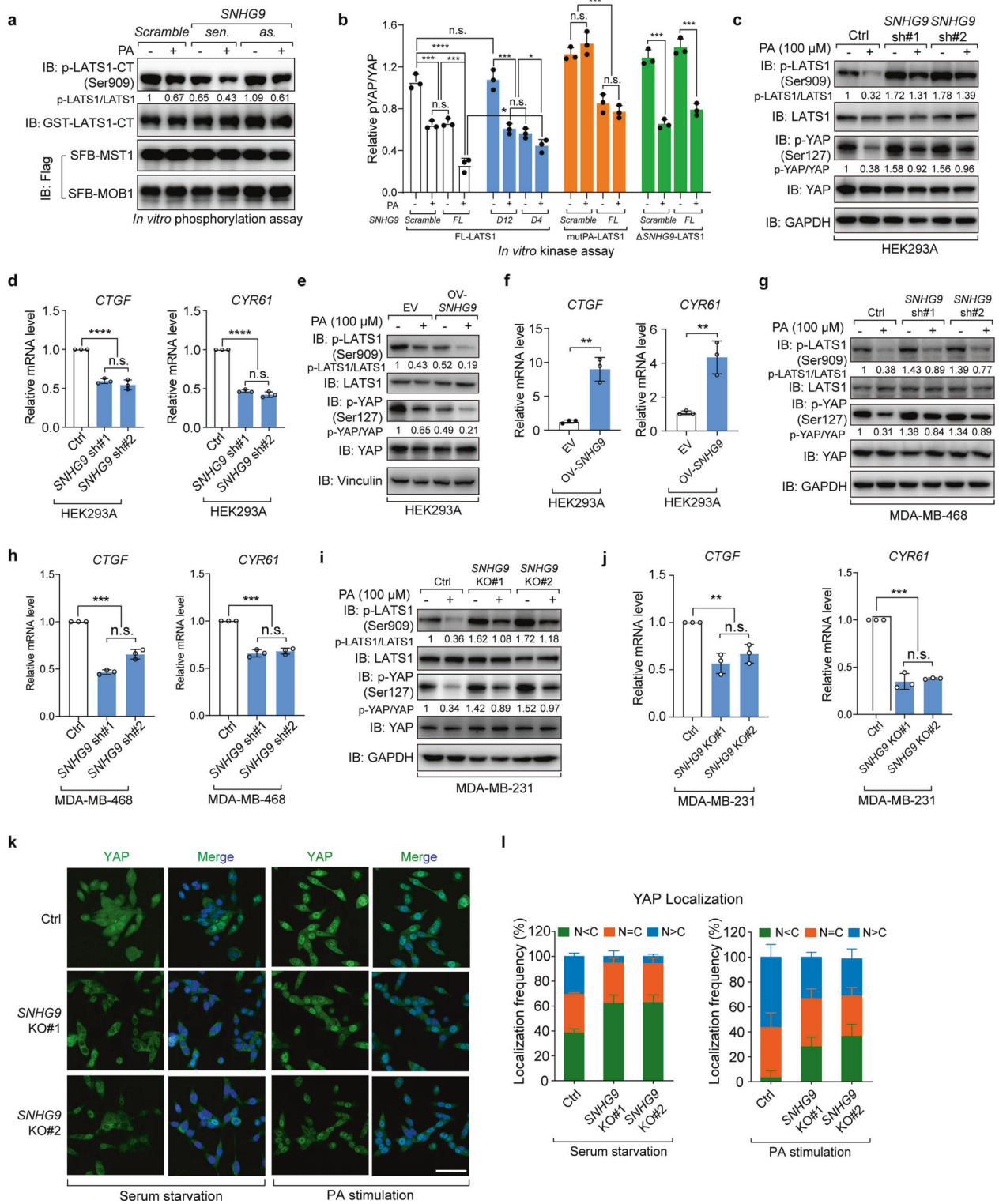
Consistent with our previous study,²¹ LATS1 directly interacted with PA (Fig. 2m). Mutating the PA-binding sites of LATS1 (mutPA-LATS1-C1: the lysine and arginine in 617–622 aa, 657–662 aa, 734–739 aa were mutated to alanine, see also Supplementary information, Fig. S3d) did not affect the LATS1–*SNHG9* interaction (Supplementary information, Fig. S3d), consistent with the fact that the PA- and *SNHG9*-binding sites on LATS1 are separated from each other. Since PA is a vital regulator of the Hippo pathway by inhibiting the LATS1 kinase activity via direct interaction,²¹ we examined the role of *SNHG9* in regulating the LATS1–PA interaction using lipid strips. Of note, *SNHG9* increased the PA enrichment by LATS1 (Fig. 2n), which depended on the association between *SNHG9* and LATS1 (Supplementary information, Fig. S3e). Further studies showed that PA reciprocally increased the levels of LATS1 enriched by *SNHG9* (Fig. 2o), which was abolished by either deleting the PA-binding region on *SNHG9* or mutating the PA-binding sites on LATS1²¹ (Fig. 2p). Therefore, these results indicate that *SNHG9*/PA/LATS1 may form a complex. We next performed protein pull-down-coupled PA detection assay to quantify PA molecules enriched by LATS1 in the presence or absence of *SNHG9*. When excess PA molecules were added to the experimental system, we found that

the abundance of LATS1-associated PA could still be significantly increased by the addition of *SNHG9* (Supplementary information, Fig. S3f), suggesting that *SNHG9* could recruit additional PA into the complex. Results with LATS1/*SNHG9* mutants (Δ *SNHG9*-LATS1 (deletion of *SNHG9* binding domain, 762–794 aa), *SNHG9*-D12 (deletion of LATS1-binding motif, the first and second loop of *SNHG9*, 7–43 nt) also support the presence of multiple PA molecules in the complex, which may be separately bound by LATS1 or *SNHG9*.

Consistent with our previous findings,²¹ PA directly bound the C-terminal of LATS1 and disrupted the LATS1–MOB1 interaction (Fig. 2q). Moreover, we found that *SNHG9* directly interacted with LATS1 (Fig. 2a, b). Therefore, we hypothesized that *SNHG9* may promote the inhibitory effect of PA on the LATS1–MOB1 complex formation. As expected, overexpression of *SNHG9* impaired the LATS1–MOB1 association (Fig. 2r; Supplementary information, Fig. S3g), while knocking down the expression of *SNHG9* attenuated PA's inhibition of the LATS1–MOB1 formation (Fig. 2s). In summary, *SNHG9* could form a complex with PA and LATS1, further impairing the LATS1–MOB1 association.

***SNHG9* promotes PA-mediated LATS1 inactivation**

As MOB1 is required for LATS1 kinase activity,²⁹ *SNHG9* may regulate LATS1 kinase activity. Since the autophosphorylation of LATS1 at S909 determines its kinase activity,^{29,32} we next examined the regulation of LATS1 S909 phosphorylation by *SNHG9* and PA. In vitro kinase assay showed that *SNHG9* and PA both inhibited LATS1 autophosphorylation at S909 (Fig. 3a). To identify the functional domains of *SNHG9* and PA in regulating LATS1 activity, LATS1 and *SNHG9* mutants were used in an in vitro kinase assay. Results showed that PA was able to inhibit full-length LATS1 (FL-LATS1) autophosphorylation at S909 and the YAP phosphorylation at S127, while PA failed to inhibit that of mutPA-LATS1 and YAP (Fig. 3b; Supplementary information, Fig. S3h). Similarly, *SNHG9* could not inhibit Δ *SNHG9*-LATS1 and YAP phosphorylation (Fig. 3b; Supplementary information, Fig. S3h). Consistently, *SNHG9*-D12 mutant, but not full-length *SNHG9* (*SNHG9*-FL) or *SNHG9*-D4 mutant, failed to inhibit the phosphorylation of LATS1 and YAP (Fig. 3b; Supplementary information, Fig. S3h). Thus, LATS1 kinase activity was inhibited by *SNHG9* and PA.



Next, we examined the role of *SNHG9* in the PA-mediated inhibition on LATS1 in vivo.²¹ Indeed, loss of *SNHG9* largely revoked PA-mediated inhibition on the phosphorylation of LATS1 and YAP in HEK293A, MDA-MB-231, and MDA-MB-468 cells (Fig. 3c, g, i; Supplementary information, Fig. S3i). Consistently, loss of *SNHG9* sequestered YAP in the cytoplasm (Fig. 3k, l) and decreased transcription of YAP target genes upon the PA treatment (Fig. 3d, h, j). This Hippo signaling alteration

was reversed when *SNHG9* was overexpressed in cells (Fig. 3e, f; Supplementary information, Fig. S3j). Similarly, restoring the expression of murine *snhg9* and human *SNHG9* in *SNHG9* KO MDA-MB-231 cells rescued the PA-mediated suppression on LATS1 phosphorylation and the expression of YAP target genes (Supplementary information, Fig. S3k–m). These results suggest that *SNHG9* plays an important role in the PA-mediated suppression of LATS1.

Fig. 3 *SNHG9* promotes PA-mediated LATS1 inactivation. **a** In vitro LATS1 phosphorylation assay using recombinant LATS1-CT, eukaryotic purified MST1, MOB1 proteins and in vitro-transcribed RNA transcripts as indicated in NETN buffer with the presence of 500 μ M ATP. Bacterially purified GST-LATS1-CT protein was used as the substrate. Immunoblots were used to detect the p-LATS1 (S909). **b** Flag-FL-LATS1, Flag-mutPA-LATS1 and Flag- Δ SNHG9-LATS1 were expressed in HEK293A cells, respectively, and purified by anti-Flag M2 magnetic beads. MOB1 and MST forming complex with above proteins were also pulled down. In vitro kinase assay was performed using above proteins, in vitro-transcribed SNHG9-FL, SNHG9-D12, SNHG9-D4 transcripts and PA as indicated in NETN buffer with 500 μ M ATP. Bacterially purified GST-YAP protein was used as the substrate. Densitometry analysis of p-YAP/YAP levels (means \pm SEM, $n = 3$ experiments) was shown. (n.s., not significant; * $P < 0.05$; *** $P < 0.001$; **** $P < 0.0001$, Student's t -test). **c, d** Knockdown of *SNHG9* largely revoked PA-mediated inhibition on the phosphorylation of LATS1 and YAP. Serum-starved wild-type and *SNHG9* KD HEK293A cells were treated with PA (100 μ M) for 1 h, and the levels of p-LATS1 (S909), p-YAP (S127) were detected using immunoblotting (**c**). Serum-starved wild-type and *SNHG9* KD HEK293A cells were treated with PA (100 μ M) for 4 h, and the expression levels of YAP target genes including *CTGF* and *CYR61* were detected by qRT-PCR (**d**). Error bars, SEM of three independent experiments (n.s., not significant; **** $P < 0.0001$, Student's t -test). **e, f** Overexpression of *SNHG9* promotes PA-mediated inhibition on the phosphorylation of LATS1 and YAP. Serum-starved wild-type and *SNHG9*-overexpressed HEK293A cells were treated with PA (100 μ M) for 1 h, and the levels of p-LATS1 (S909), p-YAP (S127) were detected using immunoblotting (**e**). Serum-starved wild-type and *SNHG9*-overexpressed HEK293A cells were treated with PA (100 μ M) for 4 h, and the expression levels of YAP target genes including *CTGF* and *CYR61* were detected by qRT-PCR (**f**). Error bars, SEM of three independent experiments (** $P < 0.01$, Student's t -test). **g, h** Knockdown of *SNHG9* largely revoked PA-mediated inhibition on the phosphorylation of LATS1 and YAP. Serum-starved wild-type and *SNHG9* KD MDA-MB-468 cells were treated with PA (100 μ M) for 1 h, and the levels of p-LATS1 (S909), p-YAP (S127) were detected using immunoblotting (**g**). Serum-starved wild-type and *SNHG9* KD MDA-MB-468 cells were treated with PA (100 μ M) for 4 h, and the expression levels of YAP target genes including *CTGF* and *CYR61* were detected by qRT-PCR (**h**). Error bars, SEM of three independent experiments (n.s., not significant; *** $P < 0.001$, Student's t -test). **i, j** Knockout of *SNHG9* largely revoked PA-mediated inhibition on the phosphorylation of LATS1 and YAP. Serum-starved wild-type and *SNHG9* KO MDA-MB-231 cells were treated with PA (100 μ M) for 1 h, and the levels of p-LATS1 (S909), p-YAP (S127) were detected using immunoblotting (**i**). Serum-starved wild-type and *SNHG9* KO MDA-MB-231 cells were treated with PA (100 μ M) for 4 h, and the expression levels of YAP target genes including *CTGF* and *CYR61* were detected by qRT-PCR (**j**). Error bars, SEM of three independent experiments (n.s., not significant; ** $P < 0.01$; *** $P < 0.001$, Student's t -test). **k, l** *SNHG9* KO largely revoked PA-mediated YAP nuclear translocation. Serum-starved wild-type and *SNHG9* KO MDA-MB-231 cells were treated with PA (100 μ M) for 1 h. Representative images of YAP subcellular localization were shown (**k**). Cells from five different fields were randomly selected and quantified for YAP localization (**l**). Scale bar, 50 μ m. Error bars, SEM of three independent experiments.

LATS1 undergoes LLPS

LATS1 forms puncta in cells (Fig. 1j). By conducting the bioinformatics analyses of the LATS1 protein sequence, we found that LATS1 is highly disordered and contains a prion-like domain (PrLD) at its N-terminus (Fig. 4a; Supplementary information, Fig. S5a). As PrLD is a theoretical domain mediating protein LLPS,^{33,34} it suggested that LATS1 might undergo LLPS (Fig. 1j). Indeed, exogenously expressed LATS1-GFP formed puncta in the cytoplasm, whereas the LATS1 mutant with PrLD deleted (Δ PrLD-LATS1) failed (Fig. 4b). Moreover, LATS1-GFP puncta underwent fusion (Fig. 4c; Supplementary information, Video S1), a highly dynamic process, as also demonstrated by the fluorescence recovery after photobleaching (FRAP) assay (Fig. 4d, e). Saponin was used to permeabilize the cells to produce holes on the membrane, removing soluble background interference to highlight phase-separated puncta.⁹ Intriguingly, LATS1-GFP puncta were still observed in HEK293A cells and remained in the cytoplasm even after saponin treatment, indicating the phase separation of LATS1 (Supplementary information, Fig. S5b). Endogenous LATS1 puncta were also observed in HEK293A and MDA-MB-231 cells using LATS1 antibody (Fig. 4f; Supplementary information, Fig. S5c, d). These findings suggest that LATS1 undergoes LLPS in cells.

To investigate the phase separation of LATS1 in vitro, we generated three LATS1-expressing constructs: FL-LATS1-GFP, Δ PrLD-LATS1-GFP, and PrLD-LATS1-GFP, respectively. As expected, the purified FL-LATS1-GFP and PrLD-LATS1-GFP proteins formed droplets in vitro, but Δ PrLD-LATS1-GFP failed (Fig. 4g). Furthermore, small droplets of LATS1-GFP fused into larger ones over time (Fig. 4h), and the formation of LATS1-GFP liquid droplets was concentration-dependent (Fig. 4i). As shown in Fig. 4j–l, small droplets fused into larger ones in vitro, and the droplets were dynamic with exchange of molecules between liquid droplets and the surrounding solution as indicated by FRAP assay.

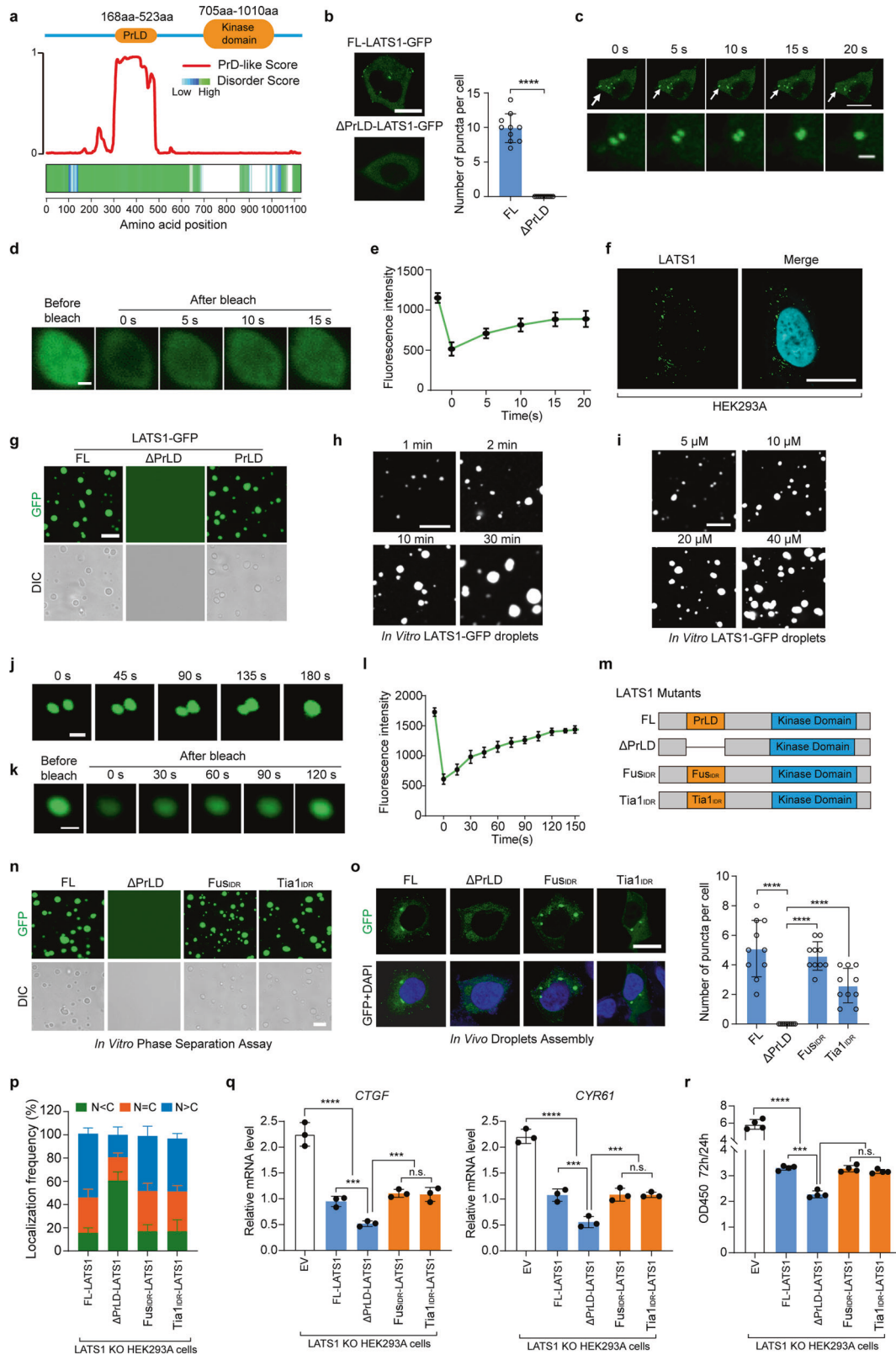
The intrinsically disordered regions (IDRs) of RNA-binding proteins can drive protein phase separation.³³ LATS1 is an RNA-binding protein and has a PrLD (equal to the IDR). To further confirm that PrLD contributes to the phase separation of LATS1,

the PrLD of LATS1 was replaced by the IDR of FUS protein or IDR of Tia1 protein. Here we named them FUS_{IDR}-LATS1 and Tia1_{IDR}-LATS1, respectively (Fig. 4m). Although deletion of PrLD prevented LATS1 phase separation (Fig. 4b, g, n, o), FUS_{IDR}-LATS1 and Tia1_{IDR}-LATS1 still underwent phase separation in vitro and in cells (Fig. 4n, o). To further examine the role of PrLD in regulating LATS1 phase separation and activity in the Hippo pathway, LATS1 FL and mutants (Δ PrLD, FUS_{IDR}, and Tia1_{IDR}) were re-expressed in LATS1 KO HEK293A cells, respectively. PrLD deletion promoted LATS1-mediated inhibition of YAP activity and cell proliferation (Fig. 4p–r; Supplementary information, Fig. S5e–g), while this effect was abolished by re-expressing FUS_{IDR}-LATS1 and Tia1_{IDR}-LATS1 (Fig. 4p–r; Supplementary information, Fig. S5e–g). These data further demonstrate that LATS1 activity is restricted by phase separation, which regulates YAP transcriptional activation.

SNHG9 promotes LATS1 phase separation

Subcellular fractionation assay by differential ultracentrifugation was used to detect heavy granule-forming proteins since proteins undergoing LLPS would be separated along with nuclei.⁹ In our study, LLPS-associated LATS1 was included in the P20 fraction (the pellet obtained at 2000 \times g), and LATS1 in the P20 fraction was a subset of total LATS1 (Fig. 5a, b). Of note, the amount of LATS1 in P20 was decreased upon RNase A treatment (Fig. 5b; Supplementary information, Fig. S6a) or in *SNHG9* knockdown cells (Fig. 5c; Supplementary information, Fig. S6b), while it was increased when *SNHG9* was overexpressed (Fig. 5d; Supplementary information, Fig. S6c). Thus, *SNHG9* likely promotes the formation of LATS1-containing heavy granules or potential liquid droplets.

We further found that overexpression of *SNHG9* enhanced LATS1 puncta formation (Fig. 5e). To confirm that LATS1 forms puncta with *SNHG9*, we overexpressed the fluorescein-labeled *SNHG9* (red) in HEK293A cells. Indeed, the transfected *SNHG9* was substantially colocalized with LATS1 and promoted LATS1 puncta formation (Fig. 5f). Consistently, LATS1 puncta formation was inhibited in *SNHG9* knockdown HEK293A cells, but it was rescued by re-expressing the fluorescein-labeled *SNHG9* (Fig. 5g, h; Supplementary information, Fig. S6d). Similarly, restoring the



expression of murine *snhg9* and human *SNHG9* in *SNHG9* KO MDA-MB-231 cells also rescued the number of LATS1 puncta (Supplementary information, Fig. S6e, f). To test whether the interaction with *SNHG9* induces LATS1 phase separation in vitro, we incubated LATS1-GFP protein with fluorescein-labeled *SNHG9*

(red). Upon mixing, LATS1 and *SNHG9* formed micrometer-sized liquid droplets (Fig. 5i). Droplet formation was observed when the protein concentration of LATS1-GFP was 0.1 μM in the presence of *SNHG9-sense*, while no droplet formed at the same protein concentration in the presence of *SNHG9-antisense* or in the

Fig. 4 LATS1 undergoes LLPS. **a** PrLD prediction of LATS1. Top, schematic illustration of LATS1 showing domains. Bottom, predictions of PrLDs and disordered regions by Prion-like Amino Acid Composition (<http://plaac.wi.mit.edu/>), IUPred (<https://iupred2a.elte.hu/>) and D2P2 algorithms (<http://d2p2.pro/>). **b** HEK293A cells transfected with FL LATS1-GFP or Δ PrLD-LATS1-GFP (0.5 μ g/well, 24-well) were analyzed by confocal microscopy. Representative pictures were shown (left panel), and the numbers of LATS1-GFP puncta per cell were counted in ten random fields (right panel). **** $P < 0.0001$, Student's t -test. Scale bar, 10 μ m. **c** Time-series fluorescence microscopy analysis of LATS1-GFP puncta. Bottom row shows zoom-in view of two fusing puncta. Scale bar, 10 μ m (top) and 1 μ m (bottom). **d** Representative micrographs of LATS1-GFP puncta before and after photobleaching. Scale bar, 0.2 μ m. **e** Quantification of fluorescence intensity recovery in the bleached region of LATS1-GFP puncta. Error bars, SEM of three independent experiments. **f** Endogenous LATS1 puncta were detected using anti-LATS1 antibody in HEK293A cells permeabilized with 0.05% saponin. Scale bar, 10 μ m. **g** Phase-separation assay of truncation mutants of LATS1 in vitro. The FL protein and PrLD fragment phase separated into liquid-like droplets, whereas Δ PrLD-LATS1-GFP failed. Scale bar, 2 μ m. **h** Small droplets fused into larger ones over time in vitro. Scale bar, 5 μ m. **i** LATS1-GFP fused into liquid droplets in a concentration-dependent manner in vitro. Scale bar, 5 μ m. **j** LATS1-GFP droplets fused during the in vitro phase separation process. Scale bar, 1 μ m. **k** The fluorescence intensity of LATS1-GFP droplets recovered after bleaching during FRAP assay. Time 0 indicates the photobleaching pulse. Scale bar, 1 μ m. **l** Quantification of fluorescence intensity recovery in the bleached region of LATS1-GFP droplets. Error bars, SEM of three independent experiments. **m** Schematic illustration of LATS1 protein and its mutants. **n** Phase-separation assay of truncation mutants of LATS1 in vitro. FL-LATS1-GFP, FUS_{IDR}-LATS1-GFP and Tia1_{IDR}-LATS1-GFP phase separated into liquid-like droplets, whereas Δ PrLD-LATS1-GFP failed. Scale bar, 2 μ m. **o** LATS1 KO HEK293A cells were transfected with FL-LATS1-GFP, Δ PrLD-LATS1-GFP, FUS_{IDR}-LATS1-GFP and Tia1_{IDR}-LATS1-GFP (0.3 μ g/well, 24-well), then the cells were analyzed by confocal microscopy. The representative pictures were shown (left panel). The numbers of puncta per cell were counted in ten random fields (right panel). **** $P < 0.0001$, Student's t -test. Scale bar, 10 μ m. **p** LATS1 KO HEK293A cells were transfected with Flag-FL-LATS1 and its mutants (Flag- Δ PrLD-LATS1, Flag-FUS_{IDR}-LATS1 and Flag-Tia1_{IDR}-LATS1), respectively, and treated with PA (100 μ M) for 1 h after serum starvation, then the subcellular localization of YAP was detected using immunofluorescence. Cells from five different fields were randomly selected and quantified for YAP localization. Error bars, SEM of three independent experiments. **q, r** LATS1 KO HEK293A cells were reconstituted with Flag-FL-LATS1, Flag- Δ PrLD-LATS1, Flag-FUS_{IDR}-LATS1 and Flag-Tia1_{IDR}-LATS1, respectively. qRT-PCR was used to detect the YAP target gene levels in indicated cells (**q**). The cell proliferation rates from 24 h to 72 h were assessed by OD density (450 nm) (**r**). Data are means \pm SEM. n.s., not significant; *** $P < 0.001$; **** $P < 0.0001$, Student's t -test.

absence of RNA (Fig. 5j). Additionally, our orthogonal experiment suggested that LATS1 underwent phase separation in a dose-dependent manner with additional *SNHG9* (Fig. 5k). The above results reveal that lncRNA *SNHG9* promotes LATS1 phase separation.

***SNHG9* and PA promote LATS1 phase separation and inhibit its activity**

Interestingly, PA also promoted LATS1 puncta formation (Fig. 6a, b). To further characterize the roles of *SNHG9* and PA in LATS1 phase separation, FL-LATS1-GFP, mutPA-LATS1-GFP, and Δ *SNHG9*-LATS1-GFP were generated and re-expressed in LATS1 KO HEK293A cells, respectively. After serum starvation, PA was used to treat the above cells with or without the transfection of *SNHG9*. Both PA and *SNHG9* promoted FL-LATS1-GFP phase separation (Fig. 6c, d). This promotion depended on their interactions with LATS1, evidenced by that *SNHG9* did not promote the phase separation of Δ *SNHG9*-LATS1-GFP, and that the phase separation of mutPA-LATS1-GFP was not promoted by PA (Fig. 6c, d).

Next, we investigated the effect of the association of *SNHG9* with PA and LATS1 on LATS1 puncta formation. *SNHG9*-FL, *SNHG9*-D12, and *SNHG9*-D4 were respectively re-expressed in *SNHG9* KD and LATS1 KO HEK293A cells with LATS1-GFP overexpression. PA was used to treat cells after serum starvation. Results showed that *SNHG9*-D12 mutant, but not *SNHG9*-FL or *SNHG9*-D4 failed to promote LATS1 phase separation (Fig. 6e, f). Meanwhile, PA promoted LATS1 phase separation in both *SNHG9*-FL- and *SNHG9* mutants-expressing cells, although the promotion effect was stronger in *SNHG9*-FL-expressing group (Fig. 6e, f). Moreover, the number of LATS1 puncta in HEK293A cells was decreased after the treatment of 1-Butanol or 2-Butanol, inhibitors of phospholipase D that catalyzes the generation of PA from phosphatidylcholine (Supplementary information, Fig. S6g). Thus, the above data further indicate that *SNHG9* and PA promote LATS1 phase separation depending on their binding with LATS1.

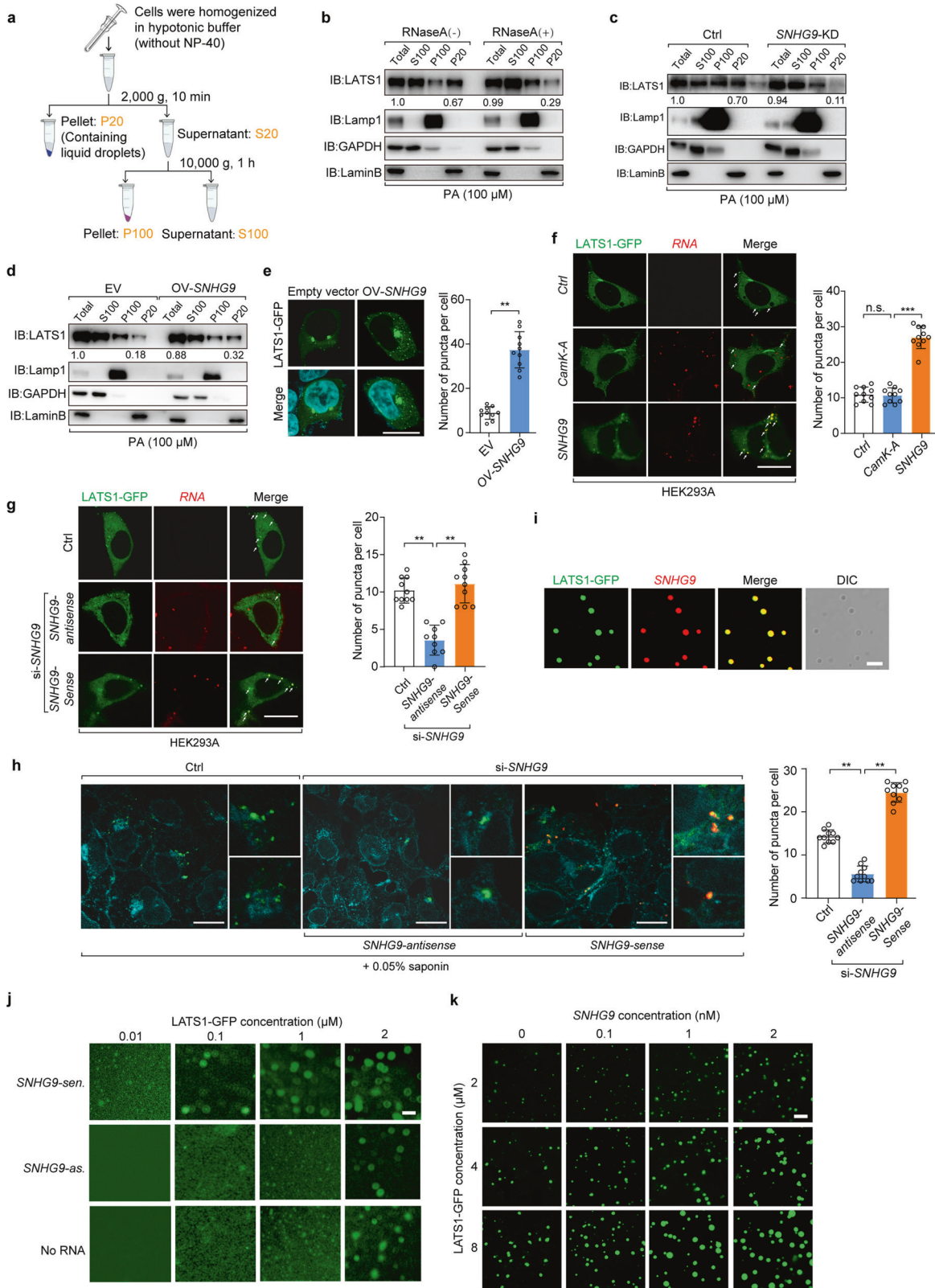
We further examined whether the activity of LATS1 was affected by its phase separation. In vitro kinase assays were performed in a physiological LLPS buffer (See Materials and Methods) with physiological ion concentration mimicking the cytoplasm. Of note, deleting the PrLD enhanced LATS1 kinase activity and abolished PA/*SNHG9*-mediated regulation in the LLPS condition

(Fig. 6g). We also examined whether LATS1 activity was affected by *SNHG9*-promoted phase separation. Interestingly, *SNHG9* reduced LATS1 phosphorylation (S909) and its kinase activity as indicated by the reduced YAP phosphorylation (S127) (Fig. 6g, h). However, *SNHG9* failed to regulate phosphorylation (S909) and kinase activity of Δ PrLD-LATS1 under the same experimental condition (Fig. 6g; Supplementary information, Fig. S6h). Unlike the FL-LATS1, treatment with PA or *SNHG9* transcript did not reduce phosphorylation or kinase activity of mutPA-LATS1 or Δ *SNHG9*-LATS1, respectively (Fig. 6i; Supplementary information, Fig. S6i). Besides, *SNHG9*-D12, but not *SNHG9*-FL or *SNHG9*-D4, failed to suppress the phosphorylation of LATS1 and YAP (Fig. 6j; Supplementary information, Fig. S6j). Taken together, these results uncover a novel role of the *SNHG9*- and PA-enhanced LATS1 phase separation in regulating LATS1 kinase activity.

To further investigate the effect of the *SNHG9*-promoted LATS1 phase separation on YAP activity and tumor cell growth, we re-expressed FL-LATS1 or Δ PrLD-LATS1 in LATS1-deficient MDA-MB-231 cells with or without *SNHG9* overexpression. Consistently, overexpression of *SNHG9* promoted YAP downstream gene transcription and cell proliferation in FL-LATS1-expressing cells (Fig. 6k–m; Supplementary information, Fig. S6k), while this was not the case in the Δ PrLD-LATS1 group (Fig. 6k–m; Supplementary information, Fig. S6k). These results suggest that *SNHG9* modulates the LATS1-YAP signaling activity by regulating LATS1 phase separation.

***SNHG9* promotes tumor growth by decreasing LATS1 activity**

Since *SNHG9* inhibited LATS1 in breast cancer cells (Fig. 1n; Supplementary information, Fig. S2f), we next examined whether *SNHG9* could promote breast cancer development through regulating the Hippo pathway. As shown in Fig. 7a–c, deletion of *SNHG9* in MDA-MB-231 cells significantly reduced xenograft tumor growth (Fig. 7a–c; Supplementary information, Fig. S7a–c). Consistently, we observed decreased proliferation and increased apoptosis as indicated by Ki-67 (the proliferation marker) and cleaved caspase-3 (the apoptosis marker) staining, respectively (Fig. 7b, c). Moreover, loss of *SNHG9* impaired angiogenesis as indicated by the staining of CD31 (an endothelial cell marker) (Fig. 7b, c). Furthermore, loss of *SNHG9* increased the phosphorylation of LATS1 (S909) and YAP (S127) (Fig. 7d), and decreased the expression of YAP downstream genes (Fig. 7e). On the other



hand, overexpression of *SNHG9* in 4T1 cells increased YAP transcriptional activation, angiogenesis, and tumor growth (Supplementary information, Fig. S7d–h). Collectively, these results demonstrate a tumor-promoting role of *SNHG9* in breast cancer development.

We also confirmed LATS1 puncta formation in xenograft tumor tissues (Fig. 7f), which were decreased upon *SNHG9* depletion (Fig. 7f). Consistently, the expression of *SNHG9* and the number of LATS1 puncta were increased during tumor development (Fig. 7g–i; Supplementary information, Fig. S7i). Moreover,

Fig. 5 *SNHG9* promotes LATS1 phase separation. **a** Schematic diagram of subcellular fractionation procedures. **b** Subcellular fractionation assay was performed in the presence or absence of RNase A (50 $\mu\text{g}/\text{mL}$) in HEK293A cells. After serum starvation, cells were treated with PA (100 μM) for 1 h. Immunoblot analysis was used to probe the cytosolic fraction (S100), membrane fraction (P100), and nuclear fraction (P20) for the indicated proteins. **c** Serum-starved wild-type HEK293A cells and *SNHG9* KD HEK293A cells, were treated with PA (100 μM) for 1 h. Then subcellular fractionation assay and immunoblot analysis were performed to show the presence of LATS1 in the nuclear fraction (P20). **d** Serum-starved wild-type HEK293A cells and HEK293A cells overexpressed with *SNHG9* were treated with PA (100 μM) for 1 h. Then subcellular fractionation assay and immunoblot analysis were performed to present LATS1 in the nuclear fraction (P20). **e** HEK293A cells with or without *SNHG9* overexpression were transfected with LATS1-GFP (0.5 $\mu\text{g}/\text{well}$, 24-well), and then analyzed by confocal microscopy. Representative pictures were shown (left panel) and the numbers of LATS1-GFP puncta per cell were counted in 10 random fields (right panel). Error bars, SEM of three independent experiments. $^{**}P < 0.01$, Student's *t*-test. Scale bar, 10 μm . **f** HEK293A cells expressing LATS1-GFP were transfected with exogenous *SNHG9* labeled with 546-UTP or *CamK-A* labeled with 546-UTP, and then analyzed by confocal microscopy. Representative pictures were shown (left panel) and the numbers of LATS1-GFP puncta per cell were counted in 10 random fields. n.s., not significant; $^{***}P < 0.001$, Student's *t*-test. Scale bar, 10 μm . **g** HEK293A cells expressing LATS1-GFP were transfected with *SNHG9* siRNA or control (Ctrl) siRNA. Cells were transfected with exogenous *SNHG9-sen.* or *SNHG9-as.* labeled with 546-UTP, and then analyzed by confocal microscopy. The representative pictures were shown (left panel) and the numbers of LATS1-GFP puncta per cell were counted in 10 random fields (right panel). $^{**}P < 0.01$, Student's *t*-test. Scale bar, 10 μm . **h** HEK293A cells expressing LATS1-GFP were transfected with *SNHG9* siRNA or control RNA. Cells were then transfected with exogenous *SNHG9-sen.* or *SNHG9-as.* labeled with 546-UTP, permeabilized with 0.05% saponin and analyzed by confocal microscopy. The representative pictures were shown (left panel) and the numbers of LATS1-GFP puncta per cell were counted in 10 random fields. $^{**}P < 0.01$, Student's *t*-test. Scale bar, 10 μm . **i** In vitro phase separation assay of LATS1-GFP and in vitro-transcribed *SNHG9* labeled with 546-UTP. Scale bar, 2 μm . **j** In vitro phase separation assay showing droplet formation of LATS1-GFP at different concentrations in the presence of 100 nM *SNHG9-sen.* (top), 100 nM *SNHG9-as.* (middle) or no RNA (bottom). Scale bar, 2 μm . **k** In vitro phase separation assay showing that *SNHG9* promotes LATS1 phase separation in a dose-dependent manner. Scale bar, 5 μm .

transcription of YAP target genes was increased (Fig. 7j; Supplementary information, Fig. S7i). These results further indicate that *SNHG9* regulates LATS1 and its target YAP in breast cancer development.

Increased *SNHG9* expression correlates with poor clinical outcomes in breast cancer patients

To determine the clinical relevance between *SNHG9* and LATS1/YAP expression, we examined their expression profiles in human breast tumors. Specifically, we examined the expression of *SNHG9* by qRT-PCR and subsequently categorized them into *SNHG9*-low and *SNHG9*-high groups by comparing their levels to the median expression. We further examined the correlation between *SNHG9* expression and tumor cell proliferation, angiogenesis, and tumor-associated macrophage by immunohistochemistry (IHC) analysis in a cohort of breast cancer tissues (SYSUCC, $n = 100$) (Fig. 8a). The expression of *SNHG9* was positively correlated with the expression of YAP, Ki-67, F4/80 (the marker of macrophages), and CD31 in breast cancer samples (Fig. 8a, b). Notably, the expression of *SNHG9* was negatively correlated with p-LATS1 (S909) but positively correlated with the number of LATS1 puncta (Fig. 8a, b) and the expression of YAP targets *CTGF* and *CYR61* in breast cancer samples (SYSUCC, $n = 100$) (Fig. 8c). These data implicate that the *SNHG9*-LATS1-YAP axis, involving the *SNHG9*-promoted LATS1 phase condensation, plays a role in human cancer development.

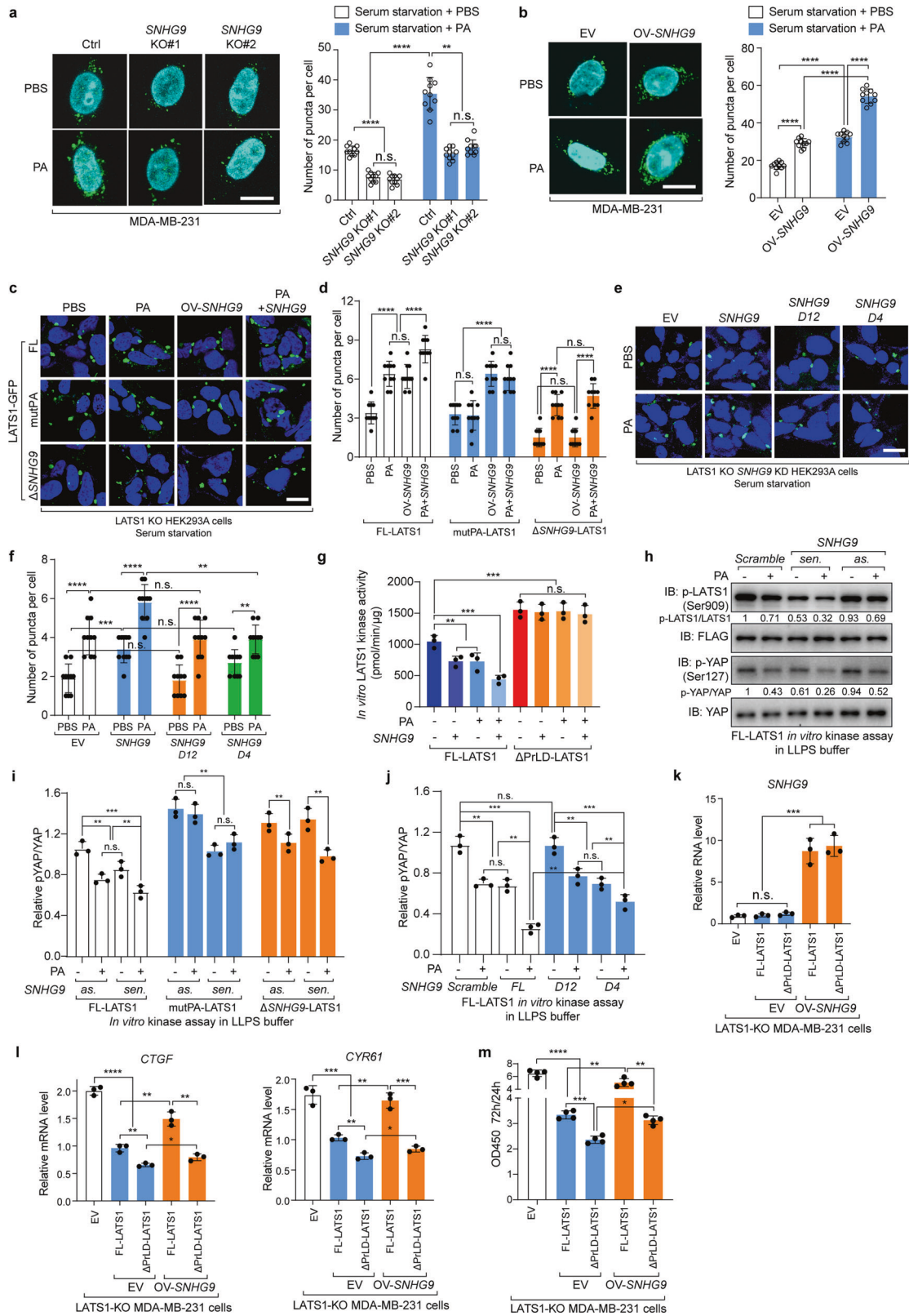
DISCUSSION

LLPS or condensation contributes to many biological processes.^{7–9} It has been reported that proteins' IDRs or electrostatic interactions drive LLPS.^{18,33,35} Excitingly, LATS1, one of the Hippo pathway core kinases, contains a PrLD in its N-terminal fragment, which drives LATS1 to undergo LLPS (Fig. 4a, b; Supplementary information, Fig. S5a). In this study, our results indicated that LATS1 underwent phase separation (Fig. 4a–l; Supplementary information, Fig. S5b–d). Intriguingly, such LATS1 phase separation is still observed when its PrLD domain was replaced by the IDR of FUS protein or IDR of Tia1 protein (Fig. 4m–o). Notably, LATS1 phase separation regulated its kinase activity; deletion of its PrLD promoted YAP cytoplasmic retention, decreased YAP downstream gene transcription, and suppressed cell proliferation (Fig. 4p–r; Supplementary information, Fig. S5e–g). Thus, our findings highlight a regulatory mechanism of LATS1 phase separation in the Hippo pathway.

RNA-binding proteins are prone to undergo LLPS,^{33,34} and RNA plays a crucial role in phase separation-related events.^{36,37} By interacting with the partner RNAs and/or other biomolecules, RNA-binding proteins form the tertiary structures, which might promote LLPS.^{33,36} RNA can shape the fluidity and viscoelasticity of LLPS droplets and lower the critical concentration required for LLPS of the RNA-binding protein^{38–40} and can also confer to the structure and physical properties of the LLPS droplets.⁴¹ In this study, we uncover that a cancer-associated lncRNA *SNHG9*, which binds and inhibits LATS1 by promoting LATS1 phase separation (Figs. 2, 3, 5, 6; Supplementary information, Figs. S3, S6), is a positive regulator of cancer cell proliferation (Fig. 6k–m). *SNHG9* gathering in LATS1 condensates can help make the droplet well-shaped and recruit additional LATS1. Notably, PA also promoted LATS1 phase separation (Fig. 6a–j; Supplementary information, Fig. S6g–j). Moreover, LATS1 kinase activity was impaired by *SNHG9*- and PA-promoted LATS1 phase separation (Fig. 6g–j; Supplementary information, Fig. S6h–j). Our study revealed a new model for signal transduction regulation in which lncRNA-mediated LATS1 phase separation regulates its kinase activity. It may provide a novel regulatory mechanism of cancer development by lncRNA via promoting phase separation.

PA is a kind of phospholipid with the capability to self-assemble as a semi-hydrophilic colloid,^{42,43} which can benefit the formation of a relatively compartmentalized coacervate. Our finding also indicated that multiple PA molecules interacted with LATS1 and *SNHG9*, and the PA involvement facilitated LATS1 LLPS. Worth mentioning, our previous study showed that *LINK-A* interacted with AKT and PIP3, facilitating AKT-PIP3 interaction and signal transduction.³ The *SNHG9*-PA-LATS1 complex also includes three different components including RNAs, lipids, and proteins; however, it is difficult to determine their delicate structures at microscale using current techniques, which could be a fascinating field in the future.

We also proposed a working model for the *SNHG9*-mediated regulation of the Hippo pathway. Under Hippo pathway-activating conditions, MST, MAP4K, TAOK, and other upstream regulators phosphorylate and activate LATS1.^{29,44} The activated LATS1 sequesters YAP in the cytoplasm by facilitating YAP phosphorylation (S127), leading to YAP degradation.⁴⁵ During cancer development, the PA-related lipid signaling is activated,²¹ and the *SNHG9* is upregulated. These factors promote LATS1 LLPS, and decrease LATS1 phosphorylation (S909) and kinase activity in the cytoplasm, resulting in YAP activation. Given that



SNHG9/*LATS1*-mediated phase separation is involved in human cancer development, further elucidation of the key biological and biophysical properties of liquid-like compartments formed by signaling regulators (e.g., kinases) in the cytoplasm might shed light on new strategies for cancer therapy.

MATERIALS AND METHODS

Tissue samples

Fresh frozen breast cancer tissues (Sun Yat-sen Cohorts) were obtained from Sun Yat-sen University Cancer Center (SYSUCC) as previously described.⁵ The study protocol was approved by the Institutional Review

Fig. 6 *SNHG9* and PA promote LATS1 phase separation and inhibit its activity. **a, b** WT and *SNHG9* KO MDA-MB-231 cells were starved overnight, treated with PA (100 μ M) for 1 h, and then analyzed by confocal microscopy. The representative pictures were shown (left panel), and the numbers of LATS1 puncta per cell were counted in ten random fields (right panel). n.s., not significant; ** $P < 0.01$; **** $P < 0.0001$, Student's *t*-test. Scale bar, 10 μ m. **c, d** FL-LATS1-GFP, mutPA-LATS1-GFP and Δ *SNHG9*-LATS1-GFP were re-expressed in LATS1 KO HEK293A cells, respectively. After serum starvation, indicated cells were treated with PA and/or transfected with *SNHG9*. Finally, all the cells were analyzed by confocal microscopy. Representative pictures were shown (**c**) and the numbers of FL-LATS1-GFP, mutPA-LATS1-GFP or Δ *SNHG9*-LATS1-GFP puncta per cell were counted, respectively, in 10 random fields (**d**). Error bars, SEM of three independent experiments. n.s., not significant; **** $P < 0.0001$, Student's *t*-test. Scale bar, 10 μ m. **e, f** *SNHG9*-FL, *SNHG9*-D12, *SNHG9*-D4 were respectively re-expressed in *SNHG9* KD and LATS1 KO HEK293A cells with LATS1-GFP overexpression. After serum starvation, indicated cells were treated with PA, and then all cells were analyzed by confocal microscopy. Representative pictures were shown (**e**) and the numbers of LATS1-GFP puncta per cell were counted, respectively, in 10 random fields (**f**). Error bars, SEM of three independent experiments. n.s., not significant; ** $P < 0.01$; *** $P < 0.001$; **** $P < 0.0001$, Student's *t*-test. Scale bar, 10 μ m. **g** Quantification of LATS1 kinase activity towards GST-YAP (pmol/min/ μ g) in the presence of the in vitro-transcribed *SNHG9* and/or PA as indicated. The levels of released phosphate ions were measured using luminescent detector (mean \pm SD; $n = 3$ biological replicates). n.s., not significant; ** $P < 0.01$; *** $P < 0.001$, Student's *t*-test. **h** Eukaryotic purified recombinant proteins Flag-FL-LATS1 was eluted by 3 \times Flag peptide. In vitro kinase assay was performed using above proteins, in vitro-transcribed *SNHG9*-*sen*/*as*. and PA as indicated in physiological LLPS buffer with 500 μ M ATP. Bacterially purified GST-YAP protein was used as the substrate. The immunoblots were used to detect p-LATS1 and p-YAP. **i** Eukaryotic purified recombinant proteins Flag-FL-LATS1, Flag-mutPA-LATS1 and Flag- Δ *SNHG9*-LATS1 were eluted by 3 \times Flag peptide. In vitro kinase assay was performed using above proteins, in vitro-transcribed *SNHG9*-*sen*/*as*. and PA as indicated in physiological LLPS buffer with 500 μ M ATP. Bacterially purified GST-YAP protein was used as the substrate. The densitometry analysis of p-YAP/YAP levels (means \pm SEM, $n = 3$ experiments) was shown. n.s., not significant; ** $P < 0.01$; *** $P < 0.001$, Student's *t*-test. **j** Eukaryotic purified recombinant protein Flag-FL-LATS1 was eluted by 3 \times Flag peptide. In vitro kinase assay was performed using FL-LATS1, in vitro-transcribed *SNHG9*-FL, *SNHG9*-D12, *SNHG9*-D4 and PA as indicated in physiological LLPS buffer with 500 μ M ATP. Bacterially purified GST-YAP protein was used as the substrate. The densitometry analysis of p-YAP/YAP levels (means \pm SEM, $n = 3$ experiments) was shown. n.s., not significant; ** $P < 0.01$; *** $P < 0.001$, Student's *t*-test. **k** qRT-PCR detection of the expression level of *SNHG9* in indicated MDA-MB-231 cell lines. Data are means \pm SEM. n.s., not significant; *** $P < 0.001$, Student's *t*-test. **l, m** LATS1 KO MDA-MB-231 cells were reconstituted with FL-LATS1 or Δ PrL-D-LATS1. The cells were transfected with *SNHG9* as indicated, and qRT-PCR was used to analyze the levels of YAP target genes (**l**). Cell proliferation rates from 24 h to 72 h were assessed by OD density (450 nm) (**m**). Data are means \pm SEM. * $P < 0.05$; ** $P < 0.01$; *** $P < 0.001$; **** $P < 0.0001$, Student's *t*-test.

Board of Sun Yat-sen University Cancer Center. All tissue samples were collected in compliance with informed consent policy. Detailed clinical information is listed in Supplementary information, Table S2.

Cloning procedures

SNHG9 (FL and mutations) and other indicated lncRNA sequences were cloned into pGEM-3Z vector (Promega) for in vitro transcription. Bacterial expression vectors for GST-LATS1 (FL and mutants) and YAP were constructed by subcloning into pGEX-4T2 vector (gift from Dr. Shanshan Liu). LATS1 expression vectors were constructed by subcloning into SFB vector using the Gateway system (Invitrogen) or pGFP-N2 (gift from QY). *SNHG9* and LATS1 were cloned into PCDH-CMV-MCS-EF1-puro vector (gift from QY) for producing lentiviruses. The pgRNA (paired-guide RNA) targeting *SNHG9* and the gRNA (guide RNA) targeting LATS1 were cloned into lentiCRISPR v2 vector for producing *SNHG9* KO MDA-MB-231 cell lines and LATS1 KO cell lines, respectively. The shRNA targeting *SNHG9* was cloned into pLKO.1-Puro vector for producing *SNHG9* KD MDA-MB-468 cell lines and *SNHG9* KD HEK293A cell lines. All single-point and deletion mutations were generated using QuikChange™ Lightning Site-Directed Mutagenesis Kit (Agilent Technologies).

Antibodies

Specific antibodies were purchased from the following commercial sources for immunoprecipitation and immunoblotting experiments: anti-p-YAP (S127) (49115, 1:1000 for IB), anti-p-LATS1 (S909) (91575, 1:1000 for IB), anti-LATS1 (34775, 1:1000 for IB and 1:100 for IP) and anti-MOB1 (13730S, 1:1000 for IB) from Cell Signaling Technology; anti-YAP monoclonal antibody (sc-101199, 1:1000 for IB) from Santa Cruz Biotechnology; anti-GAPDH (M20006, 1:5000 for IB), anti-Flag (M20008, 1:5000 for IB) and anti-GST (M20007, 1:2000 for IB) were purchased from Abmart.

For immunofluorescence, anti-YAP monoclonal antibody (sc-101199, 1:200) was purchased from Santa Cruz Biotechnology, anti-LATS1 (17049-1-AP, 1:100) was purchased from Proteintech. Alexa Fluor® 488-labeled anti-mouse secondary antibody (ab150117) and Alexa Fluor® 488-labeled anti-rabbit secondary antibody (ab150077) were purchased from Abcam.

The following antibodies were used for IHC: anti-YAP (sc-101199, 1:100) from Santa Cruz Biotechnology; anti-p-LATS1-S909 (AP0879, 1:100), anti-Ki-67 (A2094, 1:100) and anti-CD31 (A3181, 1:100) from Abclonal; anti-cleaved caspase-3 (ab2302, 1:100) from Abcam, anti-F4/80 (27044-1-AP, 1:100) from Proteintech.

Protein recombination and purification

Recombinant proteins GST-YAP, GST-LATS1 (FL and truncation mutants) were expressed in *E. coli* strain BL21-CodonPlus® (DE3)-RIPL

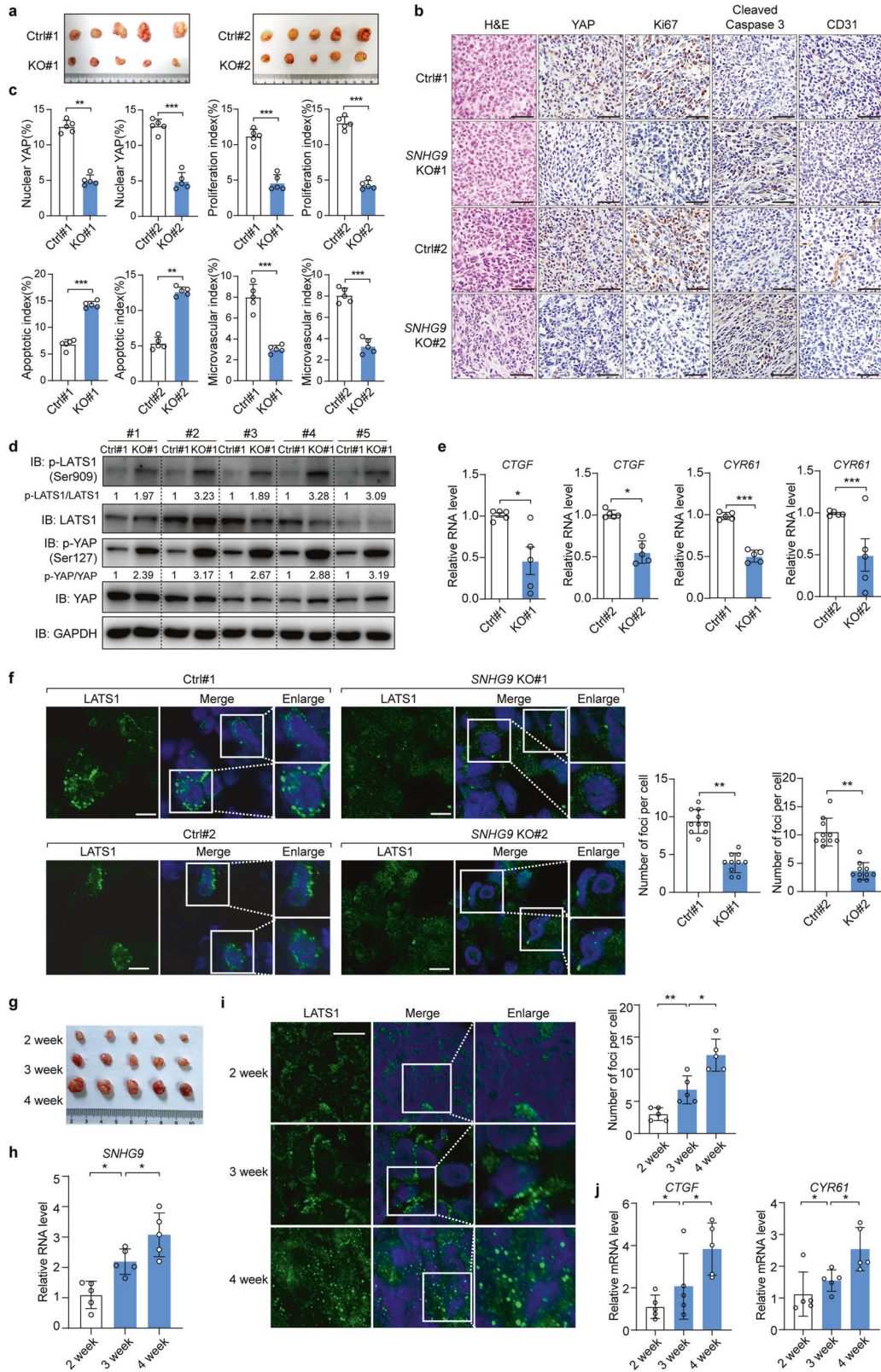
(Agilent Technologies) and purified using GST-tagged Protein Purification Kit (Sangon biotech). CD analysis was performed as previously reported.⁴⁶

Proteins used in phase separation assays were expressed in Sf9 insect cells. Cells transfected with the respective protein were grown at 28 °C in Sf-900 II SFM medium. Cell pellets were resuspended in lysis buffer (20 mM HEPES, pH 7.4, 500 mM KCl, 1 mM PMSF, 1 mM DTT, 5% glycerol). Cells were lysed by sonication. The supernatants were first purified with Ni-NTA (Sangon biotech), then washed with lysis buffer, and eluted with elution buffer (20 mM Tris-HCl, pH 7.5, 150 mM KCl, and 250 mM imidazole). Proteins were concentrated by centrifugal filtration (30 K MWCO), then purified using a SD2000 column (GE Healthcare) and stored in storage buffer (20 mM HEPES, pH 7.4, 150 mM KCl, 1 mM DTT, 5% glycerol) at -80 °C after being flash-frozen in liquid nitrogen. For proteins used in kinase assay, endogenous or recombinant LATS1 (FL and mutants) proteins were exacted from HEK293A cell lysates by immunoprecipitation.

Cell transfection, treatment and lentiviral-based gene transduction

Human breast cancer cell lines MDA-MB-231 and human embryonic kidney cell line HEK293T were purchased from American Type Culture Collection (ATCC) and characterized by Cell Line Core Facility (MD Anderson Cancer Center). HEK293A cells were kindly provided by J.-I. Park (MD Anderson Cancer Center, USA).⁴⁷ 4T1 Cells were kindly provided by Z.-J. Cai (Zhejiang University). These cell lines were maintained in Dulbecco modified essential medium (DMEM) supplemented with 10% fetal bovine serum (FBS) at 37 °C in 5% CO₂ (v/v). All cells were negatively tested for mycoplasma contamination and authenticated based on STR fingerprinting before use. No cell lines used in this study are found in the database of commonly misidentified cell lines (ICLAC and NCBI Bio sample) based on short tandem repeats (STR) profiling performed by vendors.

For KO cell line generation, lentiCRISPR v2 plasmid with modification that two U6 promoters driving the two gRNAs separately, was used to generate *SNHG9* stable KO cell lines, and lentiCRISPR v2 with LATS1 gRNA was used to generate LATS1 stable KO cell lines. The gRNAs targeting *SNHG9* and LATS1 were designed based on <http://crispr.mit.edu/> website sequence designer and cloned into lentiCRISPR v2 vector, and cell lines with best KO efficiency were used in the following functional studies. For knockdown cell line generation, shRNAs targeting *SNHG9* were designed based on Lincode SMARTpool. shRNAs were cloned into pLKO.1-Puro vector. Two shRNAs producing the best knockdown efficiency were used in the following functional studies. Detailed sequences are listed in Supplementary information, Table S3.



For lentiviral-based gene transduction, HEK293T cells were transfected with PCDH-CMV-*SNHG9* overexpression vector or pLKO.1-shRNA-*SNHG9* together with pSPAX2 and pMD2.G, and the viruses were harvested at 48 h and 72 h after transfection to transduce MDA-MB-231 cells, HEK293A cells or 4T1 cells, followed by selection with 1 µg/mL or 2 µg/mL puromycin. The

stable cell lines with *SNHG9* overexpression or *SNHG9* knockdown were screened by qRT-PCR and used for following functional studies. For labeled RNA-based cell transduction, in vitro transcribed *SNHG9* (Thermo Fisher Scientific, AM1330) was labeled with Alexa Fluor® 546 (C11404, Invitrogen).

Fig. 7 *SNHG9* promotes tumor growth by decreasing *LATS1* activity. **a** In vivo analysis of tumors in mice that were subcutaneously injected with wild-type or *SNHG9* KO MDA-MB-231 cells. **b** Representative IHC images of randomly selected tumors were shown. Scale bar, 50 μ m. **c** The relative intensities of IHC staining were quantified by Image-pro plus 6.0 software (Media Cybernetics). Error bars, SEM of three independent experiments. $**P < 0.01$; $***P < 0.001$, Student's *t*-test. **d** Immunoblot detection of p-YAP (S127) and p-LATS1 (S909) in indicated xenograft tumors. **e** qRT-PCR detection of YAP target genes, including *CTGF* and *CYR61* in indicated subcutaneous xenograft tumors. Data are means \pm SEM. $*P < 0.05$; $***P < 0.001$, Student's *t*-test. **f** Immunofluorescence analysis of *LATS1* puncta in the indicated xenograft tumor tissues permeabilized with 0.5% saponin (left panel). Scale bar, 10 μ m. The numbers of endogenous *LATS1* puncta were counted in 10 random fields (right panel). $**P < 0.01$, Student's *t*-test. **g** Mice were subcutaneously injected with wild-type MDA-MB-231 cells, and xenograft tumors were analyzed at indicated time points. **h** qRT-PCR detection of *SNHG9* expression in indicated subcutaneous xenograft tumors. Data are means \pm SD. $*P < 0.05$, Student's *t*-test. **i** Immunofluorescence analysis of *LATS1* puncta in the indicated xenograft tumor tissues permeabilized with 0.5% saponin (left panel), Scale bar, 10 μ m. The numbers of endogenous *LATS1* puncta were counted out in 10 random fields (right panel). Data are means \pm SD. $*P < 0.05$; $**P < 0.01$, Student's *t*-test. **j** qRT-PCR detection of YAP target genes, including *CTGF* and *CYR61* in indicated subcutaneous tumors. Data are means \pm SD. $*P < 0.05$, Student's *t*-test.

RNA sequencing and data analysis

Total RNA was extracted by Trizol reagent, and the quality was assessed by Bioanalyzer 2100 system (Agilent Technologies, CA, USA). 2 μ g total RNA per sample was used for RNA sequencing by rRNA depleting method. More than 15 Giga base data per sample were obtained on Illumina NovaSeq platform for following analysis.

Transcripts predicted to have coding potential by both two prediction tools (CNCL (Coding-Non-Coding-Index) (v2)/CPC (Coding Potential Calculator) (0.9-r2)) were filtered out, and transcripts without coding potential were selected as the candidate set of lncRNAs. Differential genes were analyzed by NOIseq, and $\log_2FC > 0.8$ was selected as threshold for differentially expressed transcripts. TCGA BRCA normal and tumor differentially expressed lncRNAs were analyzed, and $\log_2FC > 0.8$ was selected as threshold. RNA-seq, TCGA BRCA and our previous TNBC profiling database¹ were analyzed, and 11 overlapped lncRNA candidates were obtained.

RNA FISH assay, IHC staining, immunofluorescence staining and quantification

RNA FISH assay, IHC staining, immunofluorescence staining, and image analyses/quantification were performed as previously described.^{1-4,47}

For IHC staining, the paraffin embedded tissues were deparaffinized and rehydrated, followed by antigen retrieval. After primary and secondary antibody (listed in Antibodies section) incubation, the slide was dehydrated and stabilized with mounting medium and the images were acquired with Olympus DP72 microscope. The quantification of IHC staining density was performed by Image-Pro plus 6.0 (Media Cybernetics) and calculated on the basis of the average staining intensity and the percentage of positively stained cells. A total score of protein expression was calculated from both the percentage of positive cells and the intensity. High and low protein expression was defined using the mean score of all samples as a cutoff point. Spearman rank correlation was used for statistical analyses of the correlation between each marker and clinical stage.

RNA FISH was performed with a FISH kit (Ribobio Co.) according to the manufacturer's instruction with minor modifications. Briefly, cells with indicated treatment were fixed in 4% formaldehyde/5% acetic acid for 15 min followed by washes with PBS. The fixed cells were further treated with pepsin (1% in 10 mM HCl) and subsequent dehydration through 70%, 90% and 100% ethanol. The air-dried cells were subjected to incubation with 40 nM FISH probe (Ribobio Co.) in hybridization buffer (100 mg/mL dextran sulfate, 10% formamide in 2 \times SSC) at 80 $^{\circ}$ C for 2 min. The hybridization was performed at 55 $^{\circ}$ C for 2 h and the slide was washed with 0.1 \times SSC at 65 $^{\circ}$ C followed by dehydration through 70%, 90% and 100% ethanol. The air-dried slide was mounted with Prolong Gold Antifade Reagent with DAPI for detection.

For immunofluorescence, cells were cultured in chamber slides overnight and fixed with 3.7% formaldehyde in PBS for 10 min at 4 $^{\circ}$ C, followed by permeabilization with 0.5% Triton X-100 in PBS for 10 min. Cells were then blocked for nonspecific binding with 10% goat serum in PBS and 0.1% Tween-20 (PBST) overnight, and incubated with the indicated antibody for 1 h at room temperature, followed by incubation with Alexa Fluor-labeled secondary antibody for 30 min at room temperature. Coverslips were mounted on slides using anti-fade mounting medium with DAPI. Immunofluorescence images were acquired on a Zeiss Axio Observer Z1 fluorescence microscope. For each channel, all images were acquired with the same settings.

RNA biology assays

RNA pull-down assay, RIP assay and in vitro RNA-lipid binding coupled with dot-blot assay were performed as previously described^{1,2} with minor modifications. The cell lysates used for pull-down assay were prepared using ProteaPrep Zwitterionic Cell Lysis Kit, Mass Spec Grade (Protea[®]) with Anti-RNase, and lysis buffer supplemented with Protease Inhibitor Cocktail, Phosphatase Inhibitor Cocktail, Panobinostat, and Methylstat. The eluted protein complexes were digested by Immobilized Trypsin (Promega) and subjected to immunoblotting assay.

Cell lysis, fractionation, immunoprecipitation and immunoblotting

Cells were homogenized in RIPA buffer supplemented with Protease Inhibitor Cocktail, Phosphatase Inhibitor Cocktail, Panobinostat, and Methylstat. Lysates were cleared by centrifugation at 13,000 rpm for 15 min at 4 $^{\circ}$ C. Supernatants were analyzed for immunoblotting or for immunoprecipitation with the indicated antibodies. The blotting signals were detected using Clarity Western ECL Substrate (Bio-Rad). Cell fractionation was conducted using Subcellular Protein Fractionation Kit (Pierce).

Phase separation assay in cells

HEK293A cells expressing *LATS1*-GFP were grown on coverslips. After adhering to coverslips, cells were washed twice with PBS and fixed with 4% paraformaldehyde in PBS for 10 min. After two more washes in PBS, cells were analyzed by confocal microscopy (OLYMPUS, FV3000), and the visible puncta with diameter more than 0.5 μ m were defined as *LATS1* puncta.

Subcellular fractionation assay

RNase A (50 μ g/mL) was used to remove RNA-protein interactions in all subcellular fractionation experiments. Indicated cells were washed once in hypotonic buffer (10 mM Tris-HCl, pH 7.4, 10 mM KCl, 1.5 mM MgCl₂) and lysed using dounce homogenization. Lysates were centrifuged at 4 $^{\circ}$ C for 10 min at 2000 \times g to remove nuclei and cellular debris. Nuclear pellets were then washed 3 times in hypotonic buffer supplemented with 0.5% NP-40, resulting in the nuclear fraction (P20). Supernatants were centrifuged at 100,000 \times g for 1 h at 4 $^{\circ}$ C. The pellets were kept as the membrane fraction (P100), and the supernatants were conserved as the soluble fraction (S100). Fractionation fidelity was verified by detection of the cytosolic protein GAPDH in the soluble fraction (S100), the lysome-localized transmembrane protein Lamp1 in the insoluble, membrane fraction (P100), and Lamin B in the nuclear fraction (P20).

In vitro phase separation assay

In vitro phase separation assay was performed in storage buffer with indicated protein concentrations, and PEG8000 was also added to a final concentration of 10% (w/v). Phase separation assay was carried out on glass-bottomed dishes (NEST), sealed with optically clear adhesive film to prevent evaporation and observed under an OLYMPUS FV3000 confocal microscope equipped with 60 \times oil immersion objectives. The phase separation assay using *SNHG9* and *LATS1* was performed in a physiological LLPS buffer (20 mM Tris-HCl, pH 7.5, 15 mM NaCl, 130 mM KCl, 5 mM KH₂PO₄, 1.5 mM MgCl₂, and 1 mg/mL BSA).

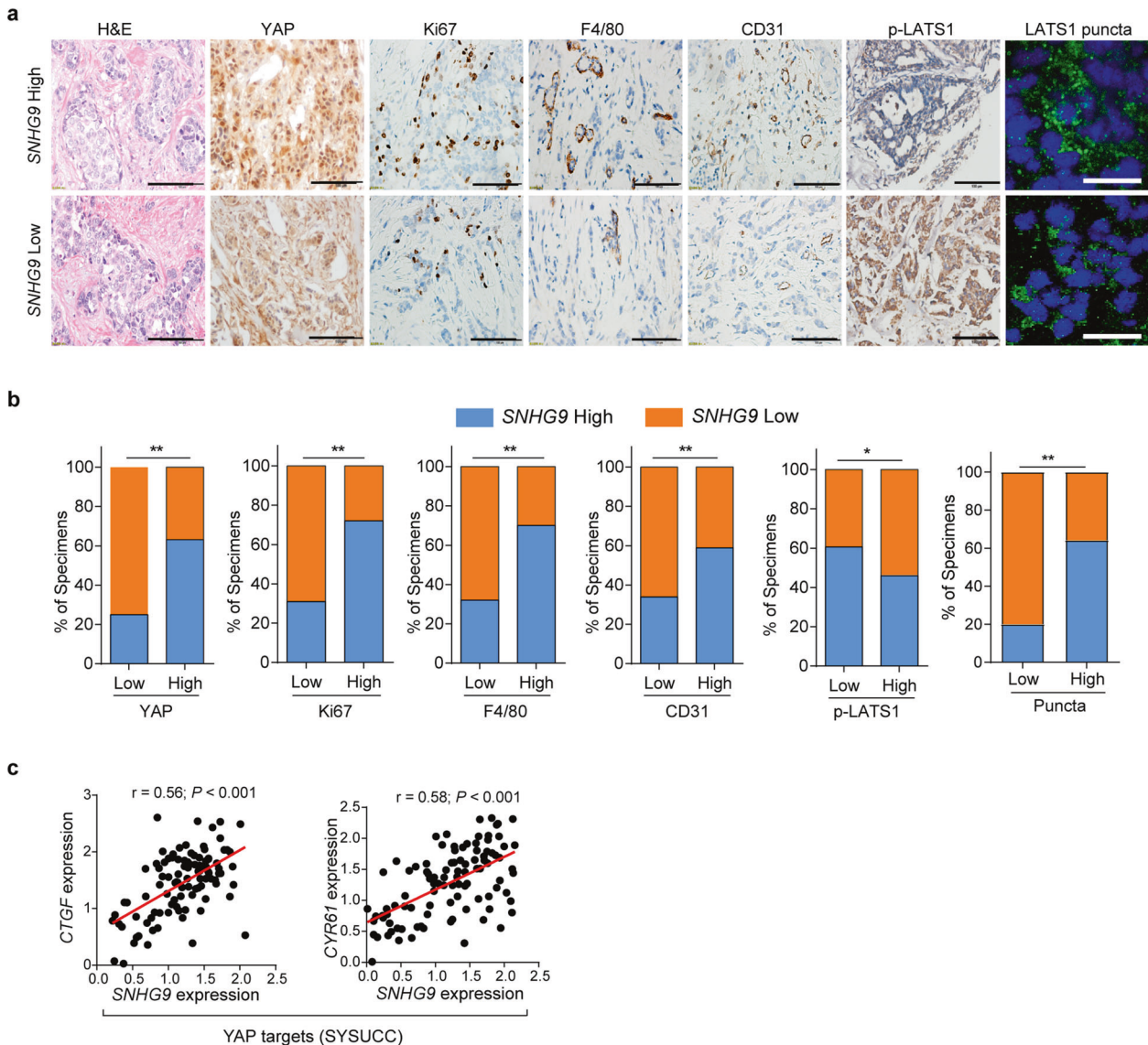


Fig. 8 Increased *SNHG9* expression correlates with poor clinical outcomes in breast cancer patients. **a** *SNHG9* level was reversely associated with p-LATS1 (S909), and positively correlated with the expression of YAP, Ki-67, F4/80, CD31 and the formation of LATS1 puncta in primary human breast cancer specimens pretreated with 0.5% saponin (Sun Yat-sen cohorts, $n = 100$). Two representative cases are shown. Scale bar, 100 μm for HE and IHC, 50 μm for IF. **b** Percentages of specimens with low or high *SNHG9* expression relative to levels of p-LATS1, YAP, Ki-67, F4/80, CD31 and LATS1 puncta are shown. * $P < 0.05$; ** $P < 0.01$, χ^2 test. **c** Correlations between expression levels of *SNHG9* and YAP target genes, including *CTGF* and *CYR61* in breast cancer tissues (Sun Yat-sen cohorts, $n = 100$). RNA levels were determined using qRT-PCR and normalized to *B2M*. The r values and P values were calculated using Pearson's correlation analysis.

FRAP

FRAP experiments were performed on an OLYMPUS FV3000 confocal microscope with a 60 \times oil immersion objective. For the in vitro experiments, droplets were photobleached with 50% laser power for 0.5 s using 488-nm lasers. Time-series images were acquired every three seconds after bleaching for 5 min. For the in vivo experiments, FRAP assays were carried out on an OLYMPUS FV3000 confocal microscope at 37 $^{\circ}\text{C}$ in a live-cell-imaging chamber. Droplets were bleached with a 488-nm laser pulse (50% intensity, 0.5 s). The recovery from photobleaching was recorded for the indicated time. Analysis of the recovery curves was carried out with Fiji/ImageJ software.

Saponin permeabilization assay

Saponin permeabilization assay was performed as previously described⁹ with minor modifications. HEK293A cells growing on coverslips were transfected with 546-labeled *SNHG9* by lipofectamine 2000 for 8 h. After washing twice with PBS, cells were stained with plasma membrane dye (5% Wheat Germ Agglutinin, Alexa Flour 350 Conjugate, Thermo Fisher) for

12 min. Then cells were washed twice with PBS and incubated with 0.05% saponin in PBS and fixed with 4% paraformaldehyde in PBS for 10 min. After two more washes in PBS, cells were imaged using confocal microscope (OLYMPUS, FV3000).

In vitro kinase assay

In vitro kinase assay was performed as previously described with minor modifications.^{5,21} FL or mutant substrate proteins were incubated with 50 μL NETN buffer containing 500 μM ATP and the indicated protein kinase for 1 h at 30 $^{\circ}\text{C}$. To test in vitro LATS1 activity, FL or mutant LATS1 protein, RNA and/or PA were incubated as indicated in NETN buffer. Resulting products were separated by SDS-PAGE and detected by immunoblotting with phospho-specific antibodies.

FL or mutant substrate proteins were incubated with 50 μL in vitro kinase assay buffer (5 mM MOPS, pH 7.2, 2.5 mM β -glycerophosphate, 1 mM EGTA, 0.4 mM EDTA, 5 mM MgCl_2 , 0.5 mM CaCl_2 , 0.03 mg/mL calmodulin, 0.05 mM DTT) containing 100 μM ATP (cold reaction) and the indicated protein kinase for 1 h at 30 $^{\circ}\text{C}$. The specific LATS1 kinase

activities were measured using a Universal Kinase Activity Kit (Beyotime).

For LATS1 kinase assay conducted in a physiological LLPS buffer, the purified FL or mutants of LATS1 protein from HEK293T cells with FL-LATS1 or its mutant overexpression, RNA and/or PA were added in a physiological LLPS buffer and incubated for 2 h at 25 °C. The enzymatic reaction was initiated by adding GST-YAP substrate and ATP and incubated for 1 h at 30 °C. Immunoblots were used to detect the p-LATS1 and p-YAP.

Detection of phosphatidic acid levels

PA levels were measured using the Total Phosphatidic Acid Assay Kit (MET-5019, Cell Biolabs) according to the manufacturer's instruction as previously reported.²¹ Briefly, 2.25 mL 1 M NaCl and 2.5 mL chloroform were added into the GST beads and mixed. Samples were centrifuged at 1500×g for 10 min and the organic phase was transferred to a glass vial, dried in a speedvac and dissolved in the Assay Buffer. Samples and the provided PA standards were transferred into a 96-well plate, and mixed with the provided Lipase Solution. The plate was incubated at 37 °C for 0.5 h. Then the Detection Enzyme Mixture solution was added into each well and the fluorescent signal was detected using a microplate reader (excitation wavelength: 530–560 nm and emission wavelength: 585–595 nm). The PA concentration was determined by subjecting the fluorescence intensity value to the standard curve and the relative PA level was normalized.

Cell viability and colony formation assay

Equal numbers of cells were plated in 96-well plates in triplicate. Cell viability was measured with MTS reagent (Promega, WI, USA). The absorbance was measured at wave length of 490 nm. For the colony formation assay, breast cancer cells were seeded into 6-well plates at a density of 500 cells/well. The cells were cultured for 14 days before they were fixed in formalin and stained with crystal violet. The colonies were counted and relative colony numbers were shown.

Three-dimensional spheroid proliferation/viability assay

Spheroid growth and invasion of parental MDA-MB-231 and its genomically edited derivative cells were conducted using the Cultrex 3D Spheroid Fluorometric Proliferation/Viability Assay kit and Cultrex 3D Spheroid BME Cell Invasion Assay kit (Trevigen), respectively, according to the vendor's instruction.

In vivo tumorigenesis study

All animal studies were approved by the Institutional Animal Care and Use Committee at our institution. Tumor cells in 30 µL growth medium (mixed with Matrigel at a 1:1 ratio) were injected subcutaneously into the flank of 6- to 8-week-old female nude or BALB/c mice using a 100 µL Hamilton Microliter™ syringe. Tumor size was measured weekly using a caliper, and tumor volume was calculated using the standard formula: $0.54 \times L \times W^2$, where L is the longest diameter and W is the shortest diameter. Mice were euthanized when they met the institutional euthanasia criteria for tumor size and overall health condition. The tumors were removed and collected for further analysis.

The amino acid sequence of PrLD-LATS1 (168–523 aa)

VQQSVNRKQSWKGSKESLVPQRHGPPLGESVAYHSESPNSQTDVGRPLSGSGI-SAFVQAHPSNGQRVNPVPPPPQVRSVTPPPPPRGTTPPPRGTTPPPSWEPNSQTK-RYSGNMEYVISRISPPVPPGAWQEGYPPPLNTSPMNPVPPNQQRGISSVPPVGRQ-PIIMQSSSKFNFPSPGRPMQNGTQDTDFMIHQNVVPAAGTVNRQPPPPYPL-TAANGQSPSALQTTGGSAAPSSYNTNGSIPQSMVMVNRNSHNMELY-NISVPLQTNWPQSSSAPAQSSPSSGHEIPTWQPNIPVRSNSFNPNLGNRASH-SANSQPSATTVTAITPAIQPVKSMRVLKPELQALAPHTPSWIPQP.

Statistics and reproducibility

The experiment was set up to use 3–5 samples/repeats per experiment/group/condition to detect a 2-fold difference with power of 80% and at the significance level of 0.05 by a two-sided test for significant studies. For immunohistochemical staining and western blotting, the representative images are shown. Each of these experiments was independently repeated for 3–5 times. Relative gene expression levels were normalized to *B2M* or *GAPDH*. Results are reported as means ± Standard Error of Mean (SEM) of at least three independent experiments. Comparisons were performed using two-tailed Student's *t*-test, χ^2 test or two-way ANOVA. For survival analysis,

the expression of indicated genes was treated as a binary variant and divided into 'high' and 'low' level. Kaplan–Meier survival curves were compared using the Gehan-Breslow test with Prism Software (GraphPad, La Jolla, CA). The experiments were not randomized. The investigators were not blinded to allocation during experiments and outcome assessment.

REFERENCES

- Xing, Z. et al. lncRNA directs cooperative epigenetic regulation downstream of chemokine signals. *Cell*. **159**, 1110–1125 (2014).
- Lin, A. et al. The LINK-A lncRNA activates normoxic HIF1alpha signalling in triple-negative breast cancer. *Nat Cell Biol*. **18**, 213–224 (2016).
- Lin, A. et al. The LINK-A lncRNA interacts with PtdIns(3,4,5)P3 to hyperactivate AKT and confer resistance to AKT inhibitors. *Nat Cell Biol*. **19**, 238–251 (2017).
- Zheng, X. et al. lncRNA wires up Hippo and Hedgehog signaling to reprogramme glucose metabolism. *EMBO J*. **36**, 3325–3335 (2017).
- Sang, L.-J. & Ju, H. Q. et al. lncRNA CamK-A regulates Ca²⁺-signaling-mediated tumor microenvironment remodeling. *Mol Cell*. **72**, 71–83.e77 (2018).
- Liu, B. et al. A cytoplasmic NF-kappaB interacting long noncoding RNA blocks IkkappaB phosphorylation and suppresses breast cancer metastasis. *Cancer Cell*. **27**, 370–381 (2015).
- Ries, R. J. et al. m(6)A enhances the phase separation potential of mRNA. *Nature*. **571**, 424–428 (2019).
- Hahn, S. Phase separation, protein disorder, and enhancer function. *Cell*. **175**, 1723–1725 (2018).
- Du, M. & Chen, Z. J. DNA-induced liquid phase condensation of cGAS activates innate immune signaling. *Science*. **361**, 704–709 (2018).
- Alberti, S., Gladfelter, A. & Mittag, T. Considerations and challenges in studying liquid-liquid phase separation and biomolecular condensates. *Cell*. **176**, 419–434 (2019).
- Clemson, C. M. et al. An architectural role for a nuclear noncoding RNA: NEAT1 RNA is essential for the structure of paraspeckles. *Mol Cell*. **33**, 717–726 (2009).
- Maharana, S. et al. Share RNA buffers the phase separation behavior of prion-like RNA binding proteins. *Science*. **360**, 918–921 (2018).
- Langdon, E. M. et al. mRNA structure determines specificity of a polyQ-driven phase separation. *Science*. **360**, 922–927 (2018).
- Yao, R. W. et al. Nascent Pre-rRNA Sorting via phase separation drives the assembly of dense fibrillar components in the human nucleolus. *Mol Cell*. **76**, 767–83.e711 (2019).
- Larson, A. G. et al. Liquid droplet formation by HP1alpha suggests a role for phase separation in heterochromatin. *Nature*. **547**, 236–240 (2017).
- Sawyer, I. A., Bartek, J. & Dundr, M. Phase separated microenvironments inside the cell nucleus are linked to disease and regulate epigenetic state, transcription and RNA processing. *Semin Cell Dev Biol*. **90**, 94–103 (2019).
- Cai, D. et al. Phase separation of YAP reorganizes genome topology for long-term YAP target gene expression. *Nat Cell Biol*. **21**, 1578–1589 (2019).
- Zhu, G. et al. Phase separation of disease-associated SHP2 mutants underlies MAPK hyperactivation. *Cell*. **183**, 1–13 (2020).
- Egea-Jimenez, A. L. & Zimmermann, P. Phospholipase D and phosphatidic acid in the biogenesis and cargo loading of extracellular vesicles. *J Lipid Res*. **59**, 1554–1560 (2018).
- Foster, D. A., Salloum, D., Menon, D. & Frias, M. A. Phospholipase D and the maintenance of phosphatidic acid levels for regulation of mammalian target of rapamycin (mTOR). *J Biol Chem*. **289**, 22583–22588 (2014).
- Han, H. et al. Regulation of the hippo pathway by phosphatidic acid-mediated lipid-protein interaction. *Mol Cell*. **72**, 328–40.e328 (2018).
- Bruntz, R. C., Lindsley, C. W. & Brown, H. A. Phospholipase D signaling pathways and phosphatidic acid as therapeutic targets in cancer. *Pharmacol Rev*. **66**, 1033–1079 (2014).
- Halder, G. & Johnson, R. L. Hippo signaling: growth control and beyond. *Development*. **138**, 9–22 (2011).
- Pan, D. The hippo signaling pathway in development and cancer. *Dev Cell*. **19**, 491–505 (2010).
- Zhao, B., Li, L., Lei, Q. & Guan, K. L. The Hippo-YAP pathway in organ size control and tumorigenesis: an updated version. *Genes Dev*. **24**, 862–874 (2010).
- Zhou, X. et al. Estrogen regulates Hippo signaling via GPER in breast cancer. *J Clin Invest*. **125**, 2123–2135 (2015).
- Harvey, K. F., Zhang, X. & Thomas, D. M. The Hippo pathway and human cancer. *Nat Rev Cancer*. **13**, 246–257 (2013).
- Yu, F. X., Zhao, B. & Guan, K. L. Hippo pathway in organ size control, tissue homeostasis, and cancer. *Cell*. **163**, 811–828 (2015).
- Ni, L., Zheng, Y., Hara, M., Pan, D. & Luo, X. Structural basis for Mob1-dependent activation of the core Mst-Lats kinase cascade in Hippo signaling. *Genes Dev*. **29**, 1416–1431 (2015).

30. Li, C. et al. A ROR1-HER3-lncRNA signalling axis modulates the Hippo-YAP pathway to regulate bone metastasis. *Nat Cell Biol.* **19**, 106–119 (2017).
31. Wang, P., Xu, J., Wang, Y. & Cao, X. An interferon-independent lncRNA promotes viral replication by modulating cellular metabolism. *Science.* **358**, 1051–1055 (2017).
32. Meng, Z. et al. MAP4K family kinases act in parallel to MST1/2 to activate LATS1/2 in the Hippo pathway. *Nat Commun.* **6**, 8357 (2015).
33. Lin, Y., Protter, D. S., Rosen, M. K. & Parker, R. Formation and maturation of phase-separated liquid droplets by RNA-binding proteins. *Mol Cell.* **60**, 208–219 (2015).
34. Wang, J. et al. A molecular grammar governing the driving forces for phase separation of prion-like RNA binding proteins. *Cell.* **174**, 688–99.e616 (2018).
35. Shin, Y. & Brangwynne, C. P. Liquid phase condensation in cell physiology and disease. *Science.* **357**, eaaf4382 (2017).
36. Fay, M. M. & Anderson, P. J. The role of RNA in biological phase separations. *J Mol Biol.* **430**, 4685–4701 (2018).
37. Daneshvar, K. et al. lncRNA DIGIT and BRD3 protein form phase-separated condensates to regulate endoderm differentiation. *Nat Cell Biol.* **22**, 1211–1222 (2020).
38. Banani, S. F., Lee, H. O., Hyman, A. A. & Rosen, M. K. Biomolecular condensates: organizers of cellular biochemistry. *Nat Rev Mol Cell Biol.* **18**, 285–298 (2017).
39. Zhang, H. et al. RNA controls PolyQ protein phase transitions. *Mol Cell.* **60**, 220–230 (2015).
40. Burke, K. A., Janke, A. M., Rhine, C. L. & Fawzi, N. L. Residue-by-residue view of in vitro FUS granules that bind the C-terminal domain of RNA polymerase II. *Mol Cell.* **60**, 231–241 (2015).
41. Langdon, E. M. & Gladfelter, A. S. A new lens for RNA localization: liquid-liquid phase separation. *Annu Rev Microbiol.* **72**, 255–271 (2018).
42. Hauser, H. & Gains, N. Spontaneous vesiculation of phospholipids: a simple and quick method of forming unilamellar vesicles. *Proc Natl Acad Sci USA.* **79**, 1683–1687 (1982).
43. Hauser, H. Mechanism of spontaneous vesiculation. *Proc Natl Acad Sci USA.* **86**, 5351–5355 (1989).
44. Meng, Z., Moroiishi, T. & Guan, K. L. Mechanisms of Hippo pathway regulation. *Genes Dev.* **30**, 1–17 (2016).
45. Hao, Y., Chun, A., Cheung, K., Rashidi, B. & Yang, X. Tumor suppressor LATS1 is a negative regulator of oncogene YAP. *J Biol Chem.* **283**, 5496–5509 (2008).
46. Micsonai, A. et al. Accurate secondary structure prediction and fold recognition for circular dichroism spectroscopy. *Proc Natl Acad Sci.* **112**, E3095–E3103 (2015).
47. Wang, W. et al. AMPK modulates Hippo pathway activity to regulate energy homeostasis. *Nat Cell Biol.* **17**, 490–499 (2015).

ACKNOWLEDGEMENTS

We thank Dr. Chao Tong (Zhejiang university) for providing Raf1-PABD-EGFP-PA sensor vector. We thank Dr. Shanshan Liu (Nanjing Drum Tower Hospital, The Affiliated Hospital of Nanjing University Medical School) for providing PGEX-4T2 vector. We also thank QY (Zhejiang University) for providing PCDH-CMV-MCS-EF1-puro and pGFP-N2 vectors. We thank XL for the help in CD assay and related bioinformatics analyses. This work was supported in part by the National Natural Science Foundation of China (81872300, 82071567, 81672791), Zhejiang Provincial Natural Science Fund for Distinguished Young Scholars of China (LR18C060002) to AL, and an NIH grant (GM126048) and an American Cancer Society Research Scholar grant (RSG-18-009-01-CCG) to WW. AL is a scholar of Thousand Youth Talents-China, a scholar of Thousand Talents-Zhejiang, a scholar of Hundred Talents-Zhejiang University.

AUTHOR CONTRIBUTIONS

AL conceived and designed the research. RHL, TT and QWG performed most of the biochemical and molecular experiments, with the assistance from XYH, CYS, JHL, ZZ, FZL, ZZY, LJS, and YZL. QWG and RHL performed the phase separation assay. TT ascertained and processed clinical specimens. ZZY conducted the bioinformatics analyses. TT, RHL, QWG, XYH, and FZL performed xenograft experiments and IHC analyses. TZ, WW, JZS, LJW, JL, QY, XL, YX, and HQJ contributed to discussion and data interpretation. WW provided reagents. JL and WW revised the manuscript. AL wrote the manuscript.

COMPETING INTERESTS

The authors declare no competing interests.

ADDITIONAL INFORMATION

Supplementary information The online version contains supplementary material available at <https://doi.org/10.1038/s41422-021-00530-9>.

Correspondence and requests for materials should be addressed to A.L.

Reprints and permission information is available at <http://www.nature.com/reprints>